

# Neural Moving Horizon Estimation for Robust Flight Control

Bingheng Wang, Zhengtian Ma, Shupeng Lai, and Lin Zhao\*

**Abstract**—Estimating and reacting to external disturbances is crucial for robust flight control of quadrotors. Existing estimators typically require significant tuning for a specific flight scenario or training with extensive ground-truth disturbance data to achieve satisfactory performance. In this paper, we propose a neural moving horizon estimator (NeuroMHE) that can automatically tune the MHE parameters modeled by a neural network and adapt to different flight scenarios. We achieve this by deriving the analytical gradients of the MHE estimates with respect to the tuning parameters, which enable a seamless embedding of an MHE as a learnable layer into the neural network for highly effective learning. Most interestingly, we show that the gradients can be obtained efficiently from a Kalman filter in a recursive form. Moreover, we develop a model-based policy gradient algorithm to train NeuroMHE directly from the trajectory tracking error without the need for the ground-truth disturbance data. The effectiveness of NeuroMHE is verified extensively via both simulations and physical experiments on a quadrotor in various challenging flights. Notably, NeuroMHE outperforms the state-of-the-art estimator with force estimation error reductions of up to 49.4% by using only a 2.5% amount of the neural network parameters. The proposed method is general and can be applied to robust adaptive control for other robotic systems.

**Index Terms**—Moving horizon estimation, Neural network, Unmanned Aerial Vehicle, Robust flight control.

## SUPPLEMENTARY MATERIAL

The source code of this work is available at <https://github.com/RCL-NUS/NeuroMHE>. The video demos can be found at <https://youtu.be/Z68zwvhL0XE>.

## I. INTRODUCTION

QUADROTORs have been increasingly engaged in various challenging tasks, such as aerial swarms [2], surveillance [3], aerial manipulation [4], and cooperative transport [5], [6]. They can suffer from strong disturbances caused by capricious wind conditions, unmodeled aerodynamics in extreme flights or tight formations [7]–[11], force interaction with environments, time-varying cable tensions from suspended payloads [12], etc. These disturbances must be compensated appropriately in control systems to avoid significant deterioration in flight performance and even crashing. However, it is generally intractable to have a portable model capable of capturing various disturbances over a wide range of complex flight scenarios. Therefore, online disturbance

Parts of this work have been presented at the 60th IEEE Conference on Decision and Control [1]. The authors are with the Department of Electrical and Computer Engineering, National University of Singapore, 117583 Singapore wangbingheng@u.nus.edu, {zhengtian, eleshla, elezhli}@nus.edu.sg.

Manuscript received XXX, 2021; revised August XXX, 2021.

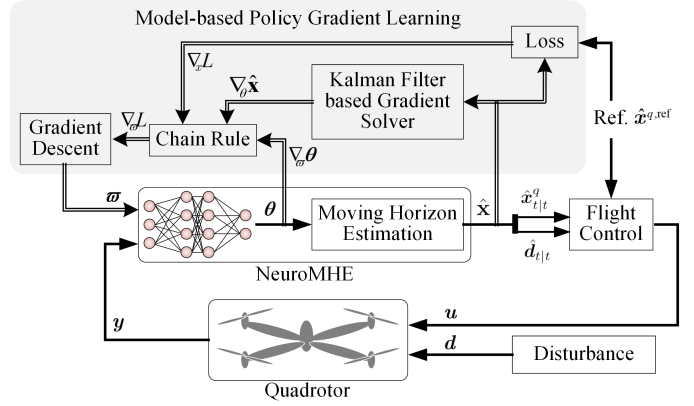


Fig. 1: An overview of NeuroMHE and learning pipelines. We fuse a neural network with an MHE to model the tuning parameters  $\theta$  which can adapt to the state-dependent noise. The neural network parameters  $\varpi$  are learned directly from the trajectory tracking error without the need for the ground-truth disturbance data. Central to our algorithm are the gradients  $\nabla_\theta \hat{x}$ , which are calculated recursively using a Kalman filter.

estimation that adapts to environments is imperative for robust flight control.

Estimating and reacting to external disturbances has long been a focus of quadrotor research. Some early works [4], [13]–[16] proposed momentum-based estimators using a stable low pass filter. Those methods depend on static disturbance assumption, and thus have limited performance against fast-changing disturbances. McKinnon et al. [17] modelled the dynamics of the disturbances as random walks and applied an unscented Kalman filter (UKF) to estimate the external disturbances. This method generally works well across different scenarios. However, its performance relies heavily on manually tuning tens of noise covariance parameters that are hard to identify in practice. In fact, the tuning process can be rather obscure and requires significant experimental efforts together with much expert knowledge of the overall system. In addition, there has been an increasing interest of utilizing deep neural networks (DNNs) for quadrotor disturbance estimation [11], [12], [18], [19]. Shi et al. [11] trained DNNs to capture the aerodynamic interaction forces between multiple quadrotors in close-proximity flight. Bauersfeld et al. proposed a hybrid estimator NeuroBEM [10] to improve the aerodynamic estimation for a single quadrotor at extreme flight. The latter combines the first-principle Blade Element Momentum model for single rotor aerodynamic modeling and a DNN for residual aerodynamic estimation. These DNN estimators generally employ a relatively large neural network model to achieve satisfactory performance. Meanwhile, their training

demands significant amounts of ground-truth disturbance data or requires particularly designed learning curricula.

Different from the above methods, we propose a neural moving horizon estimator (NeuroMHE) that can accurately estimate the external disturbances and adapt to different flight scenarios. NeuroMHE fuses a portable neural network model with an MHE and can be trained efficiently without the need for the ground-truth disturbance data. MHE is a control-theoretic estimator which solves a nonlinear optimization online using a fixed-length horizon of the most recent measurements. It is well known to have superior performance on nonlinear systems with uncertainties [20], [21]. In practice, the performance of MHE is affected by a set of weighting matrices in the cost function. These weighting matrices are tuning parameters of an MHE. They are typically chosen as the inverse of the noise covariance matrices [22]–[25]. However, these covariances often change in a complex manner and can depend on the system state [26]–[28]. To achieve satisfactory performance, a sophisticated manual tuning process is required in conventional implementation of MHE.

The proposed NeuroMHE is an auto-tuning and adaptive optimal estimator, leveraging the advantages from both advanced machine learning techniques and control-theoretic estimation algorithms. An overview of our approach is outlined in Figure 1. The tuning parameters of MHE are generated online by a neural network according to the system state, allowing for fast online adaptation to the state-dependent noise. We develop a model-based policy gradient algorithm to train the neural network parameters directly from the quadrotor trajectory tracking error. To achieve this, we perform a sensitivity analysis to analytically compute the gradients of the MHE estimates with respect to the tuning parameters. Specifically, they are derived by implicitly differentiating through the Karush-Kuhn-Tucker (KKT) conditions of the corresponding MHE optimization problem. The analytical gradients enable a seamless embedding of an MHE as a learnable layer into the neural network for highly effective learning. They allow for training NeuroMHE with powerful machine learning tools. There has been a growing interest in joining the force of control-theoretic policies and machine learning approaches, such as OptNet [29], differentiable MPC [30], and Pontryagin differentiable programming [31], [32]. Our work adds to this collection another general policy for estimation, which is of interdisciplinary interest to both robotics and machine learning communities.

Recently, there are some related works of automatically tuning MHE [33], [34]. In [33], the gradients of the MHE estimates with respect to the tuning parameters are computed via solving the inverse of a large KKT matrix, whose size is linear to the MHE horizon, and this incurs considerable computational burden for an MHE with a long horizon. In addition, the method in [34] requires the system dynamics to be linear. Our work differs from them in two key ways. The first is that our method to obtain the gradients is computationally efficient, which explores a recursive form based on a Kalman filter. The second is that the MHE optimization problem under consideration is nonlinear and general, which can be applied to robust adaptive control for other robotic systems.

We validate the effectiveness of NeuroMHE extensively via both simulations and physical experiments on a quadrotor in various challenging flights. On a real flight dataset [10], we show that compared with NeuroBEM, our method: 1) requires much less training data; 2) uses a mere 2.5% amount of the neural network parameters; and 3) achieves superior performance with force estimation error reductions of up to 49.4%. To demonstrate the benefits of generating the tuning parameters online with a neural network, we synthesize the disturbance data using the state-dependent noise. We show that the neural network-based tuning parameters can adapt to the time-varying inverse of the state-dependent noise covariance. It is also shown that NeuroMHE achieves up to 42% better trajectory tracking performance, outperforming an optimally-tuned MHE without the neural network. Finally, in the experiments, we further show that a baseline flight controller with NeuroMHE as an augmentation is able to substantially improve the robustness to challenging disturbances such as the downwash effect.

The main contributions of this paper are summarized below.

- 1) We propose NeuroMHE which fuses a neural network with an MHE to realize accurate estimation and fast online adaptation;
- 2) We develop a computationally efficient method to iteratively solve for the gradients of the MHE estimates with respect to the tuning parameters, which explores a recursive form using a Kalman filter;
- 3) We develop a model-based policy gradient algorithm to learn the neural network directly from the trajectory tracking error without the need for the ground-truth disturbance data, simultaneously improving both estimation and control performance;
- 4) By extensive comparative simulations and physical experiments, we show that NeuroMHE enjoys highly efficient training, accurate estimation, and fast adaptation to different flight scenarios.

The rest of this paper is organized as follows. Section II briefly reviews the quadrotor dynamics and the MHE problem for the disturbance estimation. Section III formulates NeuroMHE. In Section IV, we derive the analytical gradients via a sensitivity analysis. Section V develops the model-based policy gradient algorithm for training NeuroMHE without the need for the ground-truth data. Section VI extends the proposed method to handle constraints on the system state and noise. Simulation and experiment results are reported in Section VII. We conclude this paper and discuss our future work in Section VIII.

## II. PRELIMINARIES

### A. Quadrotor and Disturbance Dynamics

We model a quadrotor as a 6 degree-of-freedom (DoF) rigid body with mass  $m$  and moment of inertia  $\mathbf{J} \in \mathbb{R}^{3 \times 3}$ . Let  $\mathbf{p} \in \mathbb{R}^3$  denote the global position of Center-of-Mass (CoM) in world frame  $\mathcal{I}$ ,  $\mathbf{v} \in \mathbb{R}^3$  the velocity of CoM in  $\mathcal{I}$ ,  $\mathbf{R} \in SO(3)$

the rotation matrix from body frame  $\mathcal{B}$  to  $\mathcal{I}$ , and  $\omega \in \mathbb{R}^3$  the angular velocity in  $\mathcal{B}$ . The quadrotor model is given by:

$$\dot{\mathbf{p}} = \mathbf{v}, \quad \dot{\mathbf{v}} = m^{-1}(-mgz + \mathbf{R}\mathbf{f}\mathbf{z} + \mathbf{d}_f), \quad (1a)$$

$$\dot{\mathbf{R}} = \mathbf{R}\boldsymbol{\omega}^\times, \quad \dot{\boldsymbol{\omega}} = \mathbf{J}^{-1}(-\boldsymbol{\omega}^\times\mathbf{J}\boldsymbol{\omega} + \boldsymbol{\tau}_m + \mathbf{d}_\tau), \quad (1b)$$

where the disturbance forces  $\mathbf{d}_f = [d_{fx}; d_{fy}; d_{fz}]$  and torques  $\mathbf{d}_\tau = [d_{\tau x}; d_{\tau y}; d_{\tau z}]$  are expressed in  $\mathcal{I}$  and  $\mathcal{B}$ , respectively,  $g$  is the gravitational acceleration,  $\mathbf{z} = [0; 0; 1]$ ,  $\boldsymbol{\omega}^\times$  denotes the skew-symmetric matrix form of  $\boldsymbol{\omega}$  as an element of the Lie algebra  $so(3)$ ,  $\mathbf{f}$  and  $\boldsymbol{\tau}_m = [\tau_{mx}; \tau_{my}; \tau_{mz}]$  are the total thrust and control torques produced by the quadrotor's four motors. We define  $\mathbf{x}^q = [\mathbf{p}; \mathbf{v}; \text{vec}(\mathbf{R}); \boldsymbol{\omega}]$  as the quadrotor state where  $\text{vec}(\cdot)$  denotes the vectorization of a given matrix and  $\mathbf{u} = [f; \tau_{mx}; \tau_{my}; \tau_{mz}]$  as the control input.

Since the disturbance can come from arbitrary unknown sources (e.g., aerodynamic drag or tension force from cable-suspended payloads), a general way to model its dynamics is using random walks:

$$\dot{\mathbf{d}}_f = \mathbf{w}_f, \quad \dot{\mathbf{d}}_\tau = \mathbf{w}_\tau, \quad (2)$$

where  $\mathbf{w}_f \in \mathbb{R}^3$  and  $\mathbf{w}_\tau \in \mathbb{R}^3$  are the process noises. This model has proven sufficient to estimate unknown and time-varying disturbances [17]. We extend  $\mathbf{x}^q$  with  $\mathbf{d} = [\mathbf{d}_f; \mathbf{d}_\tau]$  to obtain  $\mathbf{x} = [\mathbf{p}; \mathbf{v}; \mathbf{d}_f; \text{vec}(\mathbf{R}); \boldsymbol{\omega}; \mathbf{d}_\tau]$  whose dynamics model can be written as:

$$\dot{\mathbf{x}} = \mathbf{f}_{\text{dyn}}(\mathbf{x}, \mathbf{u}, \boldsymbol{\omega}), \quad (3a)$$

$$\mathbf{y} = \mathbf{h}(\mathbf{x}) + \boldsymbol{\nu}, \quad (3b)$$

where  $\mathbf{f}_{\text{dyn}}$  consists of both the quadrotor rigid body dynamics (1) and the disturbance model (2),  $\mathbf{w} = [\mathbf{w}_f; \mathbf{w}_\tau]$ ,  $\mathbf{h}$  represents the noiseless measurement as a function of the state, and  $\mathbf{y}$  is the measurement subject to the noise  $\boldsymbol{\nu}$ . The model (3) will be used in MHE for estimation.

### B. Moving Horizon Estimator

MHE is a control-theoretic estimator which solves a nonlinear optimization problem online in a receding horizon manner. At time step  $t = N, N+1, \dots$ , the MHE estimator optimizes over  $N+1$  state vectors  $\mathbf{x} = \{\mathbf{x}_k\}_{k=t-N}^t$  and  $N$  process noise vectors  $\mathbf{w} = \{\mathbf{w}_k\}_{k=t-N}^{t-1}$  on the basis of  $N+1$  measurements  $\{\mathbf{y}_k\}_{k=t-N}^t$  and  $N$  control inputs  $\{\mathbf{u}_k\}_{k=t-N}^{t-1}$  collected in a sliding window of length  $N$ . Hereafter,  $\hat{\mathbf{x}} = \{\hat{\mathbf{x}}_{k|t}\}_{k=t-N}^t$  and  $\hat{\mathbf{w}} = \{\hat{\mathbf{w}}_{k|t}\}_{k=t-N}^{t-1}$  will denote the MHE estimates of  $\mathbf{x}$  and  $\mathbf{w}$ , respectively, which are to be obtained at  $t$ . The MHE optimization problem can be written as:

$$\min_{\mathbf{x}, \mathbf{w}} J = \underbrace{\frac{1}{2} \|\mathbf{x}_{t-N} - \hat{\mathbf{x}}_{t-N}\|_P^2}_{\text{arrival cost}} + \underbrace{\frac{1}{2} \sum_{k=t-N}^t \|\mathbf{y}_k - \mathbf{h}(\mathbf{x}_k)\|_{\mathbf{R}_k}^2 + \frac{1}{2} \sum_{k=t-N}^{t-1} \|\mathbf{w}_k\|_{\mathbf{Q}_k}^2}_{\text{running cost}} \quad (4a)$$

$$\text{s.t. } \mathbf{x}_{k+1} = \mathbf{f}(\mathbf{x}_k, \mathbf{u}_k, \mathbf{w}_k, \Delta t), \quad (4b)$$

where all the norms are 2-norms weighted by the positive definite matrices  $\mathbf{P}$ ,  $\mathbf{R}_k$ , and  $\mathbf{Q}_k$  in the subscript of the norms, e.g.,  $\|\mathbf{w}_k\|_{\mathbf{Q}_k}^2 = \mathbf{w}_k^T \mathbf{Q}_k \mathbf{w}_k$ ,  $\Delta t$  is the sampling time,  $\mathbf{f}(\mathbf{x}_k, \mathbf{u}_k, \mathbf{w}_k, \Delta t)$  is the discrete-time model of  $\mathbf{f}_{\text{dyn}}$  for predicting the state, and  $\hat{\mathbf{x}}_{t-N}$  is the filter priori [35] chosen as the MHE estimate  $\hat{\mathbf{x}}_{t-N|t-1}$  of  $\mathbf{x}_{t-N}$  obtained at  $t-1$ . The first term of (4a) is the so-called arrival cost, which summarizes the previous running cost before the current estimation horizon [36]. The second and third terms of (4a) constitute the most recent running cost that serves as a trade-off between minimizing the predicted measurement error and state error.

## III. FORMULATION OF NEUROMHE

### A. Problem Statement

For the MHE problem (4), the weighting matrices generally have a significant influence on  $\hat{\mathbf{x}}$ . Increasing  $\mathbf{P}$  will slow down the dynamic response of MHE to the change of the system state, leading to large estimation error [35], [36]. However, a very small  $\mathbf{P}$  will cause the MHE estimator to be unstable. If we believe that the measurement is more accurate than the model prediction based on the prior knowledge of the noise covariance, then we increase  $\mathbf{R}_k$  and decrease  $\mathbf{Q}_k$ , vice versa. Despite these rough intuitions, tuning the weighting matrices can still be a quite tedious and intricate process, since such prior knowledge is usually difficult to obtain in practice.

These weighting matrices are tuning parameters of an MHE, denoted by  $\boldsymbol{\theta}$ . The above intuitions indicate that tuning  $\boldsymbol{\theta}$  results in different MHE estimates. For a choice of  $\boldsymbol{\theta}$ , we denote the problem (4) as MHE( $\boldsymbol{\theta}$ ) and the corresponding MHE estimates as  $\hat{\mathbf{x}}(\boldsymbol{\theta})$ . If the ground-truth data of the system state is available, we can evaluate the quality of  $\hat{\mathbf{x}}(\boldsymbol{\theta})$  using a differentiable scalar loss function  $L(\hat{\mathbf{x}}(\boldsymbol{\theta}))$  built upon the estimation error. As an alternative, since the disturbance estimate from MHE will be used in a controller to compensate for the external disturbances acting on the quadrotor, we can also build  $L(\hat{\mathbf{x}}(\boldsymbol{\theta}))$  upon the trajectory tracking error to tune MHE for the purpose of control. Then, the tuning problem is to find an optimal  $\boldsymbol{\theta}^*$  such that the MHE estimates  $\hat{\mathbf{x}}(\boldsymbol{\theta}^*)$  have the minimal loss, namely that we solve

$$\min_{\boldsymbol{\theta}} L(\hat{\mathbf{x}}(\boldsymbol{\theta})) \quad (5a)$$

$$\text{s.t. } \hat{\mathbf{x}}(\boldsymbol{\theta}) \text{ is generated by MHE}(\boldsymbol{\theta}). \quad (5b)$$

However, the process noise  $\mathbf{w}$  can in fact depend on the system state, leading to the state-dependent disturbance. In that case, the performance of MHE with the fixed  $\boldsymbol{\theta}^*$  degrades substantially. For example, the aerodynamic forces generated by the downwash effect change significantly with the relative height and velocity among two quadrotors [37], [38]. This highly dynamic scenario will substantially degrade the performance of MHE with  $\boldsymbol{\theta}^*$  trained for a specific height. To address this, we are interested in making  $\boldsymbol{\theta}^*$  adaptive to the state-dependent noise while minimizing the loss.

### B. Neural MHE tuning Parameters

In practice, the relationship between the noise covariance parameters and the system state is in general difficult to model

using first principle. Given this fact, we use a neural network to model  $\theta$ :

$$\theta = f_{\varpi}(y_t), \quad (6)$$

where  $\varpi$  are the neural network parameters to be learned. The neural network takes the current measurement  $y_t$  as the input and outputs the corresponding weighting matrices for the MHE estimator (4).

We set  $y_t$  to be the input of the neural network for three reasons. First, it is natural to assume that the covariance parameters of the measurement noise depend on the current measurement  $y_t$ . Second, the covariance parameters of the process noise can also be mainly affected by the current measurement. For example, the aerodynamic force caused by the ground effect depends on the current height of a quadrotor [39] and the aerodynamic interaction forces between quadrotors in close-proximity flight are complex functions of the current relative positions and velocities [40], all these states are measurable. Third, the upper bound of  $P$  is proportional to the magnitude of the measurement noise [35], implying that  $P$  and  $y_t$  can be related.

### C. Tuning NeuroMHE via Gradient Descent

For NeuroMHE,  $\varpi$  are tuning parameters that determine the MHE estimates. Now, our tuning objective becomes learning an optimal  $\varpi^*$  that minimizes  $L(\hat{x}(\varpi))$ , i.e.,

$$\min_{\varpi} L(\hat{x}(\varpi)) \quad (7a)$$

$$\text{s.t. } \hat{x}(\varpi) \text{ is generated by NeuroMHE}(\theta(\varpi)). \quad (7b)$$

Different from the fixed  $\theta^*$  in the problem (5), here  $\theta^*(\varpi^*)$  can appropriately respond to the change of the system state, thus enabling online adaptation to the state-dependent noise.

To learn  $\varpi^*$ , we perform gradient descent on (7). The gradient of  $L(\hat{x}(\varpi))$  with respect to  $\varpi$  can be calculated using the chain rule

$$\frac{dL(\hat{x}(\varpi))}{d\varpi} = \frac{\partial L(\hat{x})}{\partial \hat{x}} \frac{\partial \hat{x}(\theta)}{\partial \theta} \frac{\partial \theta(\varpi)}{\partial \varpi}. \quad (8)$$

Figure 1 depicts the learning pipelines for training NeuroMHE. Each update of  $\varpi$  consists of a *forward pass*, where given the current  $\varpi_t$ , the weighting matrices  $\theta_t$  are generated from the neural network for MHE to obtain  $\hat{x}$ , and thus  $L(\hat{x}(\varpi_t))$  is formed, and a *backward pass*, where  $\frac{\partial L(\hat{x})}{\partial \hat{x}}$ ,  $\frac{\partial \hat{x}(\theta)}{\partial \theta}$ , and  $\frac{\partial \theta(\varpi)}{\partial \varpi}$  are computed.

In the forward pass,  $\hat{x}$  can be obtained by any numerical optimization solver. In the backward pass,  $\frac{\partial L(\hat{x})}{\partial \hat{x}}$  is straightforward to compute as  $L(\hat{x})$  is generally an explicit function of  $\hat{x}$ ; computing  $\frac{\partial \theta(\varpi)}{\partial \varpi}$  for the neural network is standardized in many existing machine learning tools. The main challenge is how to solve for  $\frac{\partial \hat{x}(\theta)}{\partial \theta}$ , the gradients of the MHE estimates with respect to  $\theta$ . This requires differentiating through the MHE problem (4) which is a nonlinear optimization. Next, we will analytically compute  $\frac{\partial \hat{x}(\theta)}{\partial \theta}$  via a sensitivity analysis and show that the analytical expressions can be obtained iteratively by proposing a Kalman Filter-based gradient solver.

### IV. ANALYTICAL GRADIENTS

In this section, we perform a sensitivity analysis to compute  $\frac{\partial \hat{x}}{\partial \theta}$  efficiently in a recursive form. Specifically, we implicitly differentiating through the KKT conditions of the MHE problem (4). The KKT conditions define a set of first-order optimality conditions which the locally optimal  $\hat{x}$  must satisfy. We associate the dual variables  $\lambda = \{\lambda_k\}_{k=t-N}^{t-1}$  with the equality constraints (4b) and denote their optimal values by  $\lambda^*$ . Then, the corresponding Lagrangian can be written as

$$\mathcal{L} = \frac{1}{2} \|\mathbf{x}_{t-N} - \hat{\mathbf{x}}_{t-N}\|_P^2 + \bar{\mathcal{L}}, \quad (9)$$

where

$$\begin{aligned} \bar{\mathcal{L}} = & \frac{1}{2} \sum_{k=t-N}^t \|\mathbf{y}_k - \mathbf{h}(\mathbf{x}_k)\|_{\mathbf{R}_k}^2 + \frac{1}{2} \sum_{k=t-N}^{t-1} \|\mathbf{w}_k\|_{\mathbf{Q}_k}^2 \\ & + \sum_{k=t-N}^{t-1} \lambda_k^T (\mathbf{x}_{k+1} - \mathbf{f}(\mathbf{x}_k, \mathbf{u}_k, \mathbf{w}_k, \Delta t)). \end{aligned}$$

The KKT conditions of the problem (4) at  $\hat{x}$ ,  $\hat{w}$ , and  $\lambda^*$  are given by

$$\begin{aligned} \nabla_{x_{t-N}} \mathcal{L} = & \mathbf{P} (\hat{\mathbf{x}}_{t-N|t} - \hat{\mathbf{x}}_{t-N}) \\ & - \mathbf{H}_{t-N}^T \mathbf{R}_{t-N} (\mathbf{y}_{t-N} - \mathbf{h}(\hat{\mathbf{x}}_{t-N|t})) \\ & - \mathbf{F}_{t-N}^T \lambda_{t-N}^* = \mathbf{0}, \end{aligned} \quad (10a)$$

$$\nabla_{x_k} \mathcal{L} = \lambda_{k-1}^* - \mathbf{H}_k^T \mathbf{R}_k (\mathbf{y}_k - \mathbf{h}(\hat{\mathbf{x}}_{k|t})) \\ - \mathbf{F}_k^T \lambda_k^* = \mathbf{0}, \quad k = t-N+1, \dots, t, \quad (10b)$$

$$\nabla_{w_k} \mathcal{L} = \mathbf{Q}_k \hat{\mathbf{w}}_{k|t} - \mathbf{G}_k^T \lambda_k^* = \mathbf{0}, \quad k = t-N, \dots, t-1, \quad (10c)$$

$$\nabla_{\lambda_k} \mathcal{L} = \hat{\mathbf{x}}_{k+1|t} - \mathbf{f}(\hat{\mathbf{x}}_{k|t}, \mathbf{u}_k, \hat{\mathbf{w}}_{k|t}, \Delta t) = \mathbf{0}, \quad k = t-N, \dots, t-1, \quad (10d)$$

where

$$\mathbf{F}_k = \frac{\partial \mathbf{f}}{\partial \hat{\mathbf{x}}_{k|t}}, \quad \mathbf{G}_k = \frac{\partial \mathbf{f}}{\partial \hat{\mathbf{w}}_{k|t}}, \quad \mathbf{H}_k = \frac{\partial \mathbf{h}}{\partial \hat{\mathbf{x}}_{k|t}}, \quad (11)$$

and  $\lambda_t^* = \mathbf{0}$  by definition.

#### A. Differential KKT Conditions of MHE

As mentioned in Section III-C, our goal is to compute  $\frac{\partial \hat{x}}{\partial \theta}$ , i.e.,

$$\frac{\partial \hat{x}}{\partial \theta} = \left\{ \frac{\partial \hat{x}_{k|t}}{\partial \theta} \right\}_{k=t-N}^t. \quad (12)$$

For this purpose, we are motivated to implicitly differentiate the KKT conditions (10) on both sides with respect to  $\theta$ . This

results in the following *differential* KKT conditions.

$$\begin{aligned} \frac{d\nabla_{x_{t-N}}\mathcal{L}}{d\theta} &= \mathbf{L}_{t-N}^{xx} \frac{\partial \hat{\mathbf{x}}_{t-N|t}}{\partial \theta} - \mathbf{P} \frac{\partial \hat{\mathbf{x}}_{t-N}}{\partial \theta} + \mathbf{L}_{t-N}^{x\theta} \\ &\quad + \mathbf{L}_{t-N}^{xw} \frac{\partial \hat{\mathbf{w}}_{t-N|t}}{\partial \theta} - \mathbf{F}_{t-N}^T \frac{\partial \boldsymbol{\lambda}_{t-N}^*}{\partial \theta} = \mathbf{0}, \end{aligned} \quad (13a)$$

$$\begin{aligned} \frac{d\nabla_{x_k}\mathcal{L}}{d\theta} &= \mathbf{L}_k^{xx} \frac{\partial \hat{\mathbf{x}}_{k|t}}{\partial \theta} + \mathbf{L}_k^{xw} \frac{\partial \hat{\mathbf{w}}_{k|t}}{\partial \theta} - \mathbf{F}_k^T \frac{\partial \boldsymbol{\lambda}_k^*}{\partial \theta} \\ &\quad + \frac{\partial \boldsymbol{\lambda}_{k-1}^*}{\partial \theta} + \mathbf{L}_k^{x\theta} = \mathbf{0}, \end{aligned} \quad (13b)$$

$$k = t - N + 1, \dots, t,$$

$$\begin{aligned} \frac{d\nabla_{w_k}\mathcal{L}}{d\theta} &= \mathbf{L}_k^{wx} \frac{\partial \hat{\mathbf{x}}_{k|t}}{\partial \theta} + \mathbf{L}_k^{ww} \frac{\partial \hat{\mathbf{w}}_{k|t}}{\partial \theta} - \mathbf{G}_k^T \frac{\partial \boldsymbol{\lambda}_k^*}{\partial \theta} \\ &\quad + \mathbf{L}_k^{w\theta} = \mathbf{0}, \quad k = t - N, \dots, t - 1, \end{aligned} \quad (13c)$$

$$\begin{aligned} \frac{d\nabla_{\lambda_k}\mathcal{L}}{d\theta} &= \frac{\partial \hat{\mathbf{x}}_{k+1|t}}{\partial \theta} - \mathbf{F}_k \frac{\partial \hat{\mathbf{x}}_{k|t}}{\partial \theta} - \mathbf{G}_k \frac{\partial \hat{\mathbf{w}}_{k|t}}{\partial \theta} = \mathbf{0}, \\ &\quad k = t - N, \dots, t - 1, \end{aligned} \quad (13d)$$

where the coefficient matrices are defined as follows:

$$\mathbf{L}_k^{xx} = \frac{\partial^2 \mathcal{L}}{\partial \hat{\mathbf{x}}_{k|t}^2}, \quad \mathbf{L}_k^{xw} = \frac{\partial^2 \mathcal{L}}{\partial \hat{\mathbf{x}}_{k|t} \partial \hat{\mathbf{w}}_{k|t}}, \quad \mathbf{L}_k^{x\theta} = \frac{\partial^2 \mathcal{L}}{\partial \hat{\mathbf{x}}_{k|t} \partial \theta}, \quad (14a)$$

$$\mathbf{L}_k^{ww} = \frac{\partial^2 \mathcal{L}}{\partial \hat{\mathbf{w}}_{k|t}^2}, \quad \mathbf{L}_k^{wx} = \frac{\partial^2 \mathcal{L}}{\partial \hat{\mathbf{w}}_{k|t} \partial \hat{\mathbf{x}}_{k|t}}, \quad \mathbf{L}_k^{w\theta} = \frac{\partial^2 \mathcal{L}}{\partial \hat{\mathbf{w}}_{k|t} \partial \theta}, \quad (14b)$$

for  $k = t - N, \dots, t$ . In (13a) and (13b),  $\frac{\partial y_{t-N}}{\partial \theta}$  and  $\frac{\partial y_k}{\partial \theta}$  are zeros as the measurements are independent of  $\theta$ . The analytical expressions of all the matrices defined in (11) and (14) can be obtained via any software package that supports symbolic computation (e.g., CasADi [41]), and their values are known from the trajectories  $\hat{\mathbf{x}}$ ,  $\hat{\mathbf{w}}$ , and  $\boldsymbol{\lambda}^*$  obtained in the forward pass. Note that  $\frac{\partial \hat{\mathbf{x}}_{t-N}}{\partial \theta}$  is also known since it is equal to  $\frac{\partial \hat{\mathbf{x}}_{t-N|t-1}}{\partial \theta}$  obtained at  $t - 1$ . We denote  $\frac{\partial \hat{\mathbf{x}}_{t-N}}{\partial \theta}$  by  $\hat{\mathbf{X}}_{t-N}$  to distinguish it from the unknown matrices  $\left\{ \frac{\partial \hat{\mathbf{x}}_{k|t}}{\partial \theta} \right\}_{k=t-N}^t$ ,  $\left\{ \frac{\partial \hat{\mathbf{w}}_{k|t}}{\partial \theta} \right\}_{k=t-N}^{t-1}$ , and  $\left\{ \frac{\partial \boldsymbol{\lambda}_k^*}{\partial \theta} \right\}_{k=t-N}^{t-1}$ . Next, we will demonstrate that these unknowns can be computed iteratively by the proposed solver.

### B. Kalman Filter-based Gradient Solver

Note that  $\mathbf{L}_{t-N}^{xx}$  in (13a) can be rewritten as  $\mathbf{L}_{t-N}^{xx} = \mathbf{P} + \bar{\mathbf{L}}_{t-N}^{xx}$  where  $\bar{\mathbf{L}}_{t-N}^{xx} = \frac{\partial^2 \bar{\mathcal{L}}}{\partial \hat{\mathbf{x}}_{t-N|t}^2}$ . Plugging this form back to (13a) makes the resulting equations of (13) similar in structure to the original KKT conditions (10). Based on this important observation, the differential KKT conditions (13) can be viewed as a new set of KKT conditions of an auxiliary MHE system whose optimal state estimates are exactly the gradients (12). As such, we first define the new state estimate, new process noise estimate, and new optimal dual variable by

$$\hat{\mathbf{X}}_{k|t} = \frac{\partial \hat{\mathbf{x}}_{k|t}}{\partial \theta}, \quad \hat{\mathbf{W}}_{k|t} = \frac{\partial \hat{\mathbf{w}}_{k|t}}{\partial \theta}, \quad \boldsymbol{\Lambda}_k^* = \frac{\partial \boldsymbol{\lambda}_k^*}{\partial \theta}, \quad (15)$$

respectively. Then, we formulate the auxiliary MHE system in the following lemma.

**Lemma 1.** Let  $\hat{\mathbf{X}} = \left\{ \hat{\mathbf{X}}_{k|t} \right\}_{k=t-N}^t$  and  $\hat{\mathbf{W}} = \left\{ \hat{\mathbf{W}}_{k|t} \right\}_{k=t-N}^{t-1}$  be optimal estimates of  $\mathbf{X} = \left\{ \mathbf{X}_k \right\}_{k=t-N}^t$  and  $\mathbf{W} = \left\{ \mathbf{W}_k \right\}_{k=t-N}^{t-1}$ , respectively, to an auxiliary MHE system:

$$\begin{aligned} \min_{\mathbf{X}, \mathbf{W}} J_2 &= \frac{1}{2} \text{Tr} \left\| \mathbf{X}_{t-N|t} - \hat{\mathbf{X}}_{t-N} \right\|_P^2 \\ &\quad + \text{Tr} \sum_{k=t-N}^t \left( \frac{1}{2} \mathbf{X}_k^T \bar{\mathbf{L}}_k^{xx} \mathbf{X}_k + \mathbf{W}_k^T \mathbf{L}_k^{wx} \mathbf{X}_k \right) \\ &\quad + \text{Tr} \sum_{k=t-N}^{t-1} \left( \frac{1}{2} \mathbf{W}_k^T \mathbf{L}_k^{ww} \mathbf{W}_k + (\mathbf{L}_k^{w\theta})^T \mathbf{W}_k \right) \\ &\quad + \text{Tr} \sum_{k=t-N}^t \left( (\mathbf{L}_k^{x\theta})^T \mathbf{X}_k \right) \end{aligned} \quad (16a)$$

$$\text{s.t. } \mathbf{X}_{k+1} = \mathbf{F}_k \mathbf{X}_k + \mathbf{G}_k \mathbf{W}_k, \quad (16b)$$

where  $\bar{\mathbf{L}}_k^{xx} = \mathbf{L}_k^{xx}$  for  $k > t - N + 1$  and  $\text{Tr}(\cdot)$  takes the trace of a given matrix. Then, they satisfy the differential KKT conditions (13).

The proof can be found in Appendix-A. Lemma 1 provides two assertions. First, the KKT conditions of (16) are the same as the differential KKT conditions (13) of the original MHE problem (4). Second,  $\hat{\mathbf{X}}$  are exactly the gradients of  $\hat{\mathbf{x}}$  with respect to  $\theta$ , and this allows us to obtain (12) by solving the auxiliary MHE system (16). For this system, there are two important properties worth noticing. The cost function (16a) is quadratic and the dynamics model (16b) is linear, making it possible to obtain  $\hat{\mathbf{X}}$  in a closed form. Instead of resorting to any numerical optimization solver, we propose a computationally efficient method to iteratively solve for  $\hat{\mathbf{X}}$  using a Kalman filter. We now present the key result in the following lemma, which is obtained using forward dynamic programming [42].

**Lemma 2.** Given the initial conditions  $\hat{\mathbf{X}}_{t-N} = \mathbf{P}_{t-N} = \mathbf{P}^{-1}$ ,  $\bar{\mathbf{X}}_{t-N} = \mathbf{P}_{t-N} \mathbf{T}_{t-N} + \hat{\mathbf{X}}_{t-N}$ , and

$$\hat{\mathbf{X}}_{t-N|t-N}^{\text{KF}} = (\mathbf{I} + \mathbf{C}_{t-N} \mathbf{S}_{t-N}) \bar{\mathbf{X}}_{t-N}, \quad (17a)$$

$$\mathbf{C}_{t-N} = (\mathbf{I} - \mathbf{P}_{t-N} \mathbf{S}_{t-N})^{-1} \mathbf{P}_{t-N}, \quad (17b)$$

where  $\mathbf{I}$  is an identity matrix with appropriate dimension,  $\mathbf{S}_{t-N} = \mathbf{L}_{t-N}^{xw} (\mathbf{L}_{t-N}^{ww})^{-1} \mathbf{L}_{t-N}^{wx} - \bar{\mathbf{L}}_{t-N}^{xx}$ , and  $\mathbf{T}_{t-N} = \mathbf{L}_{t-N}^{xw} (\mathbf{L}_{t-N}^{ww})^{-1} \mathbf{L}_{t-N}^{w\theta} - \mathbf{L}_{t-N}^{x\theta}$ , the optimal estimates  $\hat{\mathbf{X}}$  to the auxiliary MHE system (16) can be obtained iteratively through the following steps.

First, a Kalman filter (KF) is solved for  $k = t - N + 1, \dots, t$  to generate  $\left\{ \hat{\mathbf{X}}_{k|k}^{\text{KF}} \right\}_{k=t-N+1}^t$  and  $\left\{ \mathbf{C}_k \right\}_{k=t-N+1}^t$ :

$$\hat{\mathbf{X}}_{k|k-1} = \bar{\mathbf{F}}_{k-1} \hat{\mathbf{X}}_{k-1|k-1}^{\text{KF}} - \mathbf{G}_{k-1} (\mathbf{L}_{k-1}^{ww})^{-1} \mathbf{L}_{k-1}^{w\theta}, \quad (18a)$$

$$\mathbf{P}_k = \bar{\mathbf{F}}_{k-1} \mathbf{C}_{k-1} \bar{\mathbf{F}}_{k-1}^T + \mathbf{G}_{k-1} (\mathbf{L}_{k-1}^{ww})^{-1} \mathbf{G}_{k-1}^T, \quad (18b)$$

$$\mathbf{C}_k = (\mathbf{I} - \mathbf{P}_k \mathbf{S}_k)^{-1} \mathbf{P}_k, \quad (18c)$$

$$\hat{\mathbf{X}}_{k|k}^{\text{KF}} = (\mathbf{I} + \mathbf{C}_k \mathbf{S}_k) \hat{\mathbf{X}}_{k|k-1} + \mathbf{C}_k \mathbf{T}_k, \quad (18d)$$

where for  $k = t - N + 1, \dots, t - 1$ ,  $\bar{\mathbf{F}}_k = \mathbf{F}_k - \mathbf{G}_k (\mathbf{L}_k^{ww})^{-1} \mathbf{L}_k^{wx}$ ,  $\mathbf{S}_k = \mathbf{L}_k^{xw} (\mathbf{L}_k^{ww})^{-1} \mathbf{L}_k^{wx} - \bar{\mathbf{L}}_k^{xx}$ ,  $\mathbf{T}_k =$

$L_k^{xw}(L_k^{ww})^{-1}L_k^{w\theta} - L_k^{x\theta}$ , when  $k = t$ , then  $\mathbf{S}_t = -\bar{\mathbf{L}}_t^{xx}$ , and  $\mathbf{T}_t = -L_t^{x\theta}$ .

Second,  $\Lambda^* = \{\Lambda_k^*\}_{k=t-N}^{t-1}$  are generated by solving the following equation backward in time for  $k = t, \dots, t-N+1$ , starting with  $\Lambda_t^* = \mathbf{0}$ :

$$\Lambda_{k-1}^* = (\mathbf{I} + \mathbf{S}_k \mathbf{C}_k) \bar{\mathbf{F}}_k^T \Lambda_k^* + \mathbf{S}_k \hat{\mathbf{X}}_{k|k}^{\text{KF}} + \mathbf{T}_k. \quad (19)$$

Finally,  $\hat{\mathbf{X}}$  are obtained by solving

$$\hat{\mathbf{X}}_{k|t} = \hat{\mathbf{X}}_{k|k}^{\text{KF}} + \mathbf{C}_k \bar{\mathbf{F}}_k^T \Lambda_k^* \quad (20)$$

forward in time for  $k = t-N, \dots, t$ .

The proof is presented in Appendix-B. Equations in (18) represent a Kalman filter with the matrix state  $\hat{\mathbf{X}}_{k|k}^{\text{KF}}$  and zero measurement. Among them, (18a) is the state predictor, (18b) is the projection of the error covariance, (18c) is the update of the error covariance from which the Kalman gain can be obtained using the matrix inversion lemma, and (18d) is the state corrector. The use of such a Kalman filter provides the analytical gradients with a recursive form. As a result, they can be solved iteratively and very efficiently. This algorithm acts as a key component in the backward pass of training NeuroMHE, as shown in Figure 1. We summarize the procedure of solving for  $\hat{\mathbf{X}}$  using a Kalman filter in Algorithm 1.

---

**Algorithm 1:** Solving for  $\hat{\mathbf{X}}$  using a Kalman Filter

---

**Input:** The trajectories  $\hat{\mathbf{x}}$ ,  $\hat{\mathbf{w}}$ , and  $\Lambda^*$  generated by solving the MHE problem (4), the trajectory of the control input  $\mathbf{u}$ , the gradient of the filter priori  $\hat{\mathbf{X}}_{t-N}$ , and the matrices in (11) and (14) for constructing the auxiliary MHE system (16);

```

1  def Kalman_Filter_based_Gradient_Solver:
2       $\triangleright$  implementation of Lemma 2
3      Set  $\hat{\mathbf{X}}_{t-N|t-N}^{\text{KF}}$  and  $\mathbf{C}_{t-N}$  using equation (17);
4      for  $k \leftarrow t-N+1$  to  $t$  do
5           $\triangleright$  Kalman Filter
6          Update  $\mathbf{C}_k$  and  $\hat{\mathbf{X}}_{k|k}^{\text{KF}}$  using equation (18);
7           $\triangleright$  forward recursion
8      end for
9      Set  $\Lambda_t^* = \mathbf{0}$ ;
10     for  $k \leftarrow t$  to  $t-N+1$  do
11         Update  $\Lambda_{k-1}^*$  using equation (19);
12          $\triangleright$  backward recursion
13     end for
14     for  $k \leftarrow t-N$  to  $t$  do
15         Update  $\hat{\mathbf{X}}_{k|t}$  using equation (20);
16          $\triangleright$  forward recursion
17     end for
18     return  $\{\hat{\mathbf{X}}_{k|t}\}_{k=t-N}^t$ 
19 Return:  $\frac{\partial \hat{\mathbf{x}}}{\partial \theta} = \hat{\mathbf{X}}$   $\triangleright$  due to Lemma 1

```

---

## V. MODEL-BASED POLICY GRADIENT ALGORITHM

In this section, we propose a model-based policy gradient algorithm to train NeuroMHE via reinforcement learning (RL).

This algorithm enables the neural network parameters  $\varpi$  to be learned directly from the trajectory tracking error without the need for the ground-truth disturbance data.

To achieve this goal, we consider the robust flight controller

$$\mathbf{u}_t = \mathbf{u} \left( \mathbf{x}_t^{q,\text{ref}}, \hat{\mathbf{x}}_{t|t} \right), \quad (21)$$

which can enforce the quadrotor to track the reference trajectory  $\mathbf{x}_t^{q,\text{ref}}$  in the presence of the disturbances. The estimate  $\hat{\mathbf{x}}_{t|t}$  of the current extended state  $\mathbf{x}_t$ , consisting of the estimates of  $\mathbf{x}_t^q$  and  $\mathbf{d}_t$ , is generated online by solving the MHE problem (4) based on the dynamics model (3) and the neural network (6). Here, the controller (21) is expressed in a general form and is applicable to various control algorithms. For instance, one can use the current disturbance estimate  $\hat{\mathbf{d}}_{t|t}$  as an augmentation in a geometric flight controller [43] to compensate for  $\mathbf{d}_t$  as much as possible. If  $\hat{\mathbf{d}}_{t|t}$  converges to the ground-truth  $\mathbf{d}_t$ , then the compensation will be better and this improves the trajectory tracking performance. From this intuition, one can build the loss function using the estimation error  $\|\hat{\mathbf{d}}_{t|t} - \mathbf{d}_t\|$ . However, the precise value of  $\mathbf{d}_t$  is very hard to obtain in practice. Given this difficulty, we instead build the loss using a sequence of the trajectory tracking errors accumulated over one MHE horizon:

$$L(\hat{\mathbf{x}}) = \alpha \sum_{k=t-N}^t \left\| \hat{\mathbf{x}}_{t|t}^q - \mathbf{x}_k^{q,\text{ref}} \right\|_{\mathbf{W}_e}^2, \quad (22)$$

where  $\alpha$  is a positive coefficient and  $\mathbf{W}_e$  is a positive-definite weighting matrix. The loss (22) shows that we train NeuroMHE in closed-loop and  $\hat{\mathbf{d}}_{t|t}$  is estimated for the purpose of robust flight control.

In training, we perform gradient descent to update  $\varpi$ . We first obtain the analytical gradients  $\frac{\partial \hat{\mathbf{x}}}{\partial \theta}$  using Algorithm 1, then compute  $\frac{\partial L(\hat{\mathbf{x}})}{\partial \hat{\mathbf{x}}}$  and  $\frac{\partial \theta(\varpi)}{\partial \hat{\mathbf{x}}}$  from the loss (22) and the neural network  $\mathbf{f}_{\varpi}$ , finally apply the chain rule (8) to obtain the gradient  $\frac{dL(\hat{\mathbf{x}})}{d\varpi}$ . We summarize the procedures of training NeuroMHE using the proposed model-based policy gradient RL in Algorithm 2 where  $L_{\text{mean}}$  is the mean value of the loss (22) over one training episode with the duration  $T_{\text{episode}}$ .

## VI. CONSTRAINED NEUROMHE

Our method can be conveniently extended to the case where constraints on the system state and the process noise should be respected to ensure flight safety. Without loss of generality, we consider the following constraints for  $k \in [t-N, t]$ :

$$g_{k,i}(\mathbf{x}_k, \mathbf{w}_k) \leq 0, i = 1, \dots, n. \quad (23)$$

A straightforward and common practice for constrained MHE is to enforce (23) to be hard constraints, as shown below:

$$\min_{\mathbf{x}, \mathbf{w}} J \quad (24a)$$

$$\text{s.t. } \mathbf{x}_{k+1} = \mathbf{f}(\mathbf{x}_k, \mathbf{u}_k, \mathbf{w}_k, \Delta t), \quad (24b)$$

$$g_{k,i}(\mathbf{x}_k, \mathbf{w}_k) \leq 0, i = 1, \dots, n, \quad (24c)$$

We denote  $\hat{\mathbf{x}}_c$  and  $\hat{\mathbf{w}}_c$  as the optimal estimates of  $\hat{\mathbf{x}}$  and  $\mathbf{w}$ , respectively, to the constrained MHE problem (24). Similar to

**Algorithm 2:** Model-based Policy Gradient RL

---

**Input:** The quadrotor reference trajectory  $\mathbf{x}^{q,\text{ref}}$  and the learning rate  $\varepsilon$

**Initialization:**  $\boldsymbol{\varpi}_0$

**Loss:**  $L(\hat{\mathbf{x}})$  in (22)

1 **while**  $L_{\text{mean}}$  not converged **do**

2   **for**  $t \leftarrow 0$  to  $T_{\text{episode}}$  **do**

3     Obtain  $\boldsymbol{\theta}_t$  using the neural network parameterization  $\mathbf{f}_{\boldsymbol{\varpi}_t}(\mathbf{y}_t)$ ;

4     Solve for  $\hat{\mathbf{x}}$  from the current MHE system (4);  
    ▷ using any numerical optimization solver

5     Obtain  $\mathbf{u}_t$  using the control law (21);

6     Implement  $\mathbf{u}_t$  to the quadrotor to update  $\mathbf{y}_t$ ;

7     Obtain  $\frac{\partial \hat{\mathbf{x}}}{\partial \boldsymbol{\theta}}$  using Algorithm 1 given  $\hat{\mathbf{x}}$ ;

8     Obtain  $\frac{\partial L(\hat{\mathbf{x}})}{\partial \boldsymbol{\varpi}}$  from the loss function  $L(\hat{\mathbf{x}})$ ;

9     Obtain  $\frac{\partial \boldsymbol{\theta}(\boldsymbol{\varpi})}{\partial \boldsymbol{\varpi}}$  from the neural network  $\mathbf{f}_{\boldsymbol{\varpi}_t}$ ;  
    ▷ using any machine learning tool

10    Apply the chain rule (8) to obtain  $\frac{dL(\hat{\mathbf{x}})}{d\boldsymbol{\varpi}}$ ;

11    Update  $\boldsymbol{\varpi}_t$  using gradient-based optimization;

12   **end for**

13 **end while**

---

(4),  $\hat{\mathbf{x}}_c$  can also be denoted as  $\hat{\mathbf{x}}_c(\boldsymbol{\theta})$ . This method, however, leads to several implementation difficulties for computing the gradients  $\frac{\partial \hat{\mathbf{x}}_c}{\partial \boldsymbol{\theta}}$ . When differentiating the KKT conditions of (24) with respect to  $\boldsymbol{\theta}$ , we need to identify all the active constraints  $g_{k,i}(\mathbf{x}_k, \mathbf{w}_k) = 0$ , which can be numerically challenging. Moreover, the discontinuous switch between inactive and active inequality constraints may incur numerical instability in learning. Instead of treating (23) as hard constraints, we draw inspiration from interior-point methods to softly penalize (23) in the cost function of the MHE problem (4) by using logarithm barrier functions, i.e.,

$$\min_{\mathbf{x}, \mathbf{w}} J - \delta \sum_{k=t-N}^t \sum_{i=1}^n \ln(-g_{k,i}(\mathbf{x}_k, \mathbf{w}_k)) \quad (25a)$$

$$\text{s.t. } \mathbf{x}_{k+1} = \mathbf{f}(\mathbf{x}_k, \mathbf{u}_k, \mathbf{w}_k, \Delta t), \quad (25b)$$

where  $\delta$  is a positive barrier parameter.

Compared with (24), the optimal estimates  $\hat{\mathbf{x}}$  to the soft-constrained MHE problem (25) is now determined by both  $\boldsymbol{\theta}$  and  $\delta$ , denoted by  $\hat{\mathbf{x}}(\boldsymbol{\theta}, \delta)$ . As  $\delta \rightarrow 0$ , we have  $\hat{\mathbf{x}}(\boldsymbol{\theta}, \delta) \rightarrow \hat{\mathbf{x}}_c(\boldsymbol{\theta})$  which is a well-known property of interior-point methods [44], and then we obtain  $\frac{\partial \hat{\mathbf{x}}(\boldsymbol{\theta}, \delta)}{\partial \boldsymbol{\theta}} \rightarrow \frac{\partial \hat{\mathbf{x}}_c(\boldsymbol{\theta})}{\partial \boldsymbol{\theta}}$ . This shows that by setting  $\delta > 0$  to be sufficiently small, we can utilize  $\frac{\partial \hat{\mathbf{x}}(\boldsymbol{\theta}, \delta)}{\partial \boldsymbol{\theta}}$  to approximate  $\frac{\partial \hat{\mathbf{x}}_c(\boldsymbol{\theta})}{\partial \boldsymbol{\theta}}$  with arbitrary accuracy, and this allows for applying Algorithm 1 to calculate  $\frac{\partial \hat{\mathbf{x}}(\boldsymbol{\theta}, \delta)}{\partial \boldsymbol{\theta}}$ . As such, by parameterizing  $\boldsymbol{\theta}$  in (25) with the neural network (6), we can train the soft-constrained NeuroMHE (25) using Algorithm 2.

## VII. EXPERIMENTS

We validate the effectiveness of NeuroMHE in both numerical and physical experiments on a quadrotor for robust flight

control. Specifically, we aim to show the following features of our approach. First, NeuroMHE enjoys computationally efficient training and it can achieve better force estimation performance than a state-of-the-art estimator. Second, a stable NeuroMHE can be trained directly from the trajectory tracking error with fast online adaptation to the state-dependent disturbance. Third, NeuroMHE is able to improve the robustness of a real quadrotor against strong disturbances such as the sudden payload change and the downwash effect.

In our experiments, we set the quadrotor state  $\mathbf{x}^q$  to be the output of the augmented system (3), which is measurable in most cases such as using onboard sensors and motion capture systems. To generate  $\boldsymbol{\theta}$  online that are adaptive to the state-dependent noise, we construct a multi-layer perceptron (MLP) network, the architecture of which is depicted in Figure 2. The

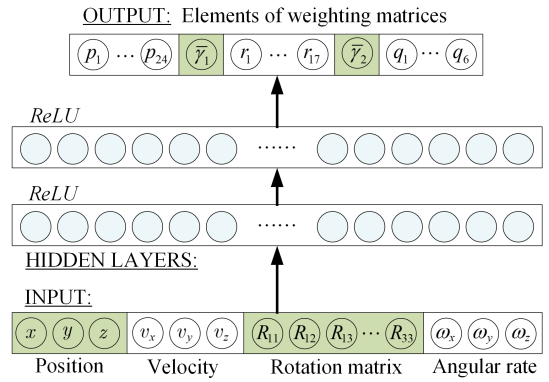


Fig. 2: Architecture of the neural network for modeling the MHE tuning parameters.

MLP takes the current measurement  $\mathbf{y}_t$  as the input that will go through two hidden layers, and then outputs all the elements in  $\boldsymbol{\theta}$ . We use rectified linear unit (ReLU)  $\phi(x) = \max(x, 0)$  as the activation function in the hidden layers. In general, neural networks with ReLU converge faster in training than those with saturating nonlinear functions such as  $\tanh(\cdot)$  [45] and demonstrate superior function approximation ability. With these settings, we can express the neural network  $\mathbf{f}_{\boldsymbol{\varpi}}$  as

$$\mathbf{f}_{\boldsymbol{\varpi}}(\mathbf{y}_t) = \mathbf{A}_o \phi(\mathbf{A}_1 \phi(\mathbf{A}_2 \phi(\mathbf{A}_1 \mathbf{y}_t + \mathbf{b}_1) + \mathbf{b}_2) + \mathbf{b}_o, \quad (26)$$

where  $\{\mathbf{A}_o, \mathbf{A}_1, \mathbf{A}_2\}$  are the weighting matrices,  $\{\mathbf{b}_o, \mathbf{b}_1, \mathbf{b}_2\}$  are the bias vectors, and all of them are denoted as the neural network parameters  $\boldsymbol{\varpi}$  to be learned.

For the MHE problem (4), we introduce two forgetting factors  $\gamma_{1,2} \in (0, 1)$  in  $\mathbf{R}_k$  and  $\mathbf{Q}_k$  to account for the historical data within the horizon, such that  $\mathbf{R}_k = \gamma_1^{t-k} \mathbf{R}_t$  and  $\mathbf{Q}_k = \gamma_2^{t-1-k} \mathbf{Q}_{t-1}$ . We set  $\mathbf{P} \in \mathbb{R}^{24 \times 24}$ ,  $\mathbf{R}_t \in \mathbb{R}^{18 \times 18}$ , and  $\mathbf{Q}_{t-1} \in \mathbb{R}^{6 \times 6}$  to be diagonal matrices, which is viable in practice [26], [46], [47]. Since the learning problem (7) is non-convex with respect to  $\boldsymbol{\theta}$ ,  $\boldsymbol{\theta}(\boldsymbol{\varpi})$  usually arrives at one of its local optima after learning. To reduce the number of the local optima, the first diagonal element in  $\mathbf{R}_t$  is fixed at 100. Then, we train the MLP (26) to tune the remaining 47 diagonal elements and the two forgetting factors, which are collected in the vector  $\boldsymbol{\theta} = [P_{1:24}, \gamma_1, R_{1:17}, \gamma_2, Q_{1:6}]$ . To ensure  $\mathbf{P}$ ,  $\mathbf{R}_t$ , and  $\mathbf{Q}_{t-1}$  are positive definite and  $\gamma_{1,2}$  lie in the range  $(0, 1)$ ,

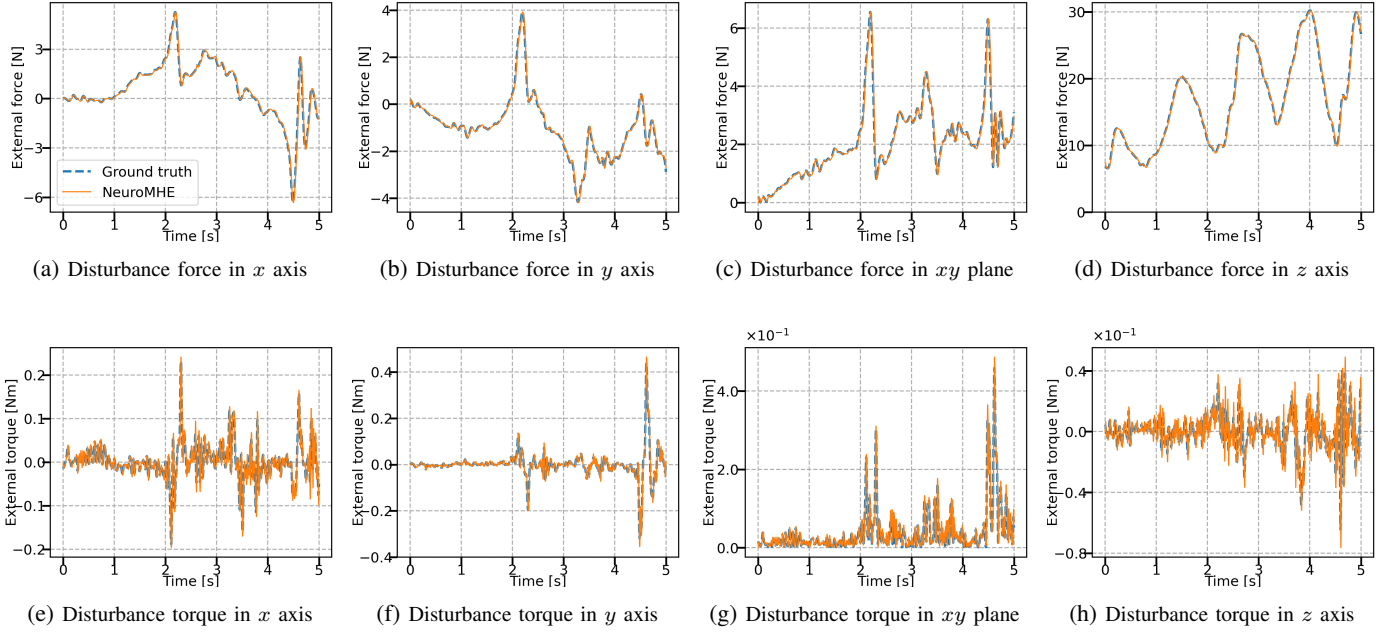


Fig. 3: Evaluation of the force and torque estimation of NeuroMHE on the same test dataset as in [10]. At  $t = 0$ , the initial guess of the disturbance used in the arrival cost is set to be  $\hat{d}_0 = [0; 0; mg; 0; 0; 0]$  since the quadrotor initially hovers at around 2.15 m. Figures 3c and 3g are obtained by plotting  $d_{fx,y} = \sqrt{d_{fx}^2 + d_{fy}^2}$  and  $d_{\tau_{xy}} = \sqrt{d_{\tau_x}^2 + d_{\tau_y}^2}$ , respectively.

we parameterize the diagonal elements as  $P_{1:24} = \varsigma + p_{1:24}^2$ ,  $R_{1:17} = \varsigma + r_{1:17}^2$ , and  $Q_{1:6} = \varsigma + q_{1:6}^2$ , respectively, with  $\varsigma > 0$ , and use two sigmoid functions to parameterize  $\gamma_1$  and  $\gamma_2$  as  $\gamma_{1,2} = (1 + \exp(-\bar{\gamma}_{1,2}))^{-1}$ . Therefore, the output of the MLP (26) becomes  $\Theta = [p_{1:24}, \bar{\gamma}_1, r_{1:17}, \bar{\gamma}_2, q_{1:6}] \in \mathbb{R}^{49}$ , as shown in Figure 2. In this case, we need to modify the chain rule (8) in the form of  $\frac{dL}{d\varpi} = \frac{\partial L}{\partial \dot{\varpi}} \frac{\partial \dot{\varpi}}{\partial \varpi} \frac{\partial \varpi}{\partial \Theta} \frac{\partial \Theta}{\partial \varpi}$  to account for the above parameterization.

We program our approach in Python where `ipopt` in CasADi [41] is used to solve the MHE problem (4). The MLP network model (26) is built in PyTorch [48] and is trained using Adam [49].

#### A. Efficient Learning for Accurate Estimation

In this simulation, we compare NeuroMHE with the state-of-the-art estimator NeuroBEM to demonstrate the first feature. This is done on a real flight dataset [10]. Since the ground-truth disturbance data can be obtained using the dataset and the dynamics model (1), we train NeuroMHE from the estimation error. Specifically, we use Algorithm 1 to compute the gradients  $\frac{\partial \dot{\varpi}}{\partial \Theta}$ , build the loss function  $L$  using the estimation error, and apply gradient descent to update the neural network parameters  $\varpi$ . The ground-truth disturbance forces and torques are computed by

$$d_f = m \mathbf{R}^T (\mathbf{a}_v + g \mathbf{z}), \quad d_\tau = \mathbf{J} \mathbf{a}_\omega + \omega^\times \mathbf{J} \omega, \quad (27)$$

where  $\mathbf{J} = \text{diag}(2.52, 2.14, 4.36) \times 10^{-3} \text{ kg m}^2$  and  $m = 0.752 \text{ kg}$  are the same as in [10],  $\mathbf{a}_v$  and  $\mathbf{a}_\omega$  are the linear

<sup>1</sup>In practical implementation, we customize the loss function to suit the typical training procedure in PyTorch. Specifically, we define  $L_{\text{pytorch}} = \frac{\partial L}{\partial \dot{\varpi}} \frac{\partial \dot{\varpi}}{\partial \varpi} \frac{\partial \varpi}{\partial \Theta}$  as the loss function for training the neural network (26) such that  $\frac{dL_{\text{pytorch}}}{d\varpi} = \frac{dL}{d\varpi}$ .

and angular accelerations given in the dataset. Here,  $d_f$  and  $d_\tau$  include the total thrust and the control torques generated by the quadrotor motors. For NeuroMHE, the dynamics model (1) is discretized using forward Euler method with the same time step of 2.5 ms as in the dataset. To obtain  $\mathbf{y}_t$  as the input for the neural network, we integrate  $\mathbf{a}_v$  to compute the velocity, convert the quaternion to the rotation matrix, and use the position and the angular rate from the dataset. Each hidden layer of the neural network has 100 neurons. In training, we single out a piece of data with the duration of 2.5 s from a figure-8 trajectory, which is defined as a training episode and covers a wide range of velocity from  $1 \text{ m s}^{-1}$  to  $15.15 \text{ m s}^{-1}$  and multiple force spikes. In evaluation, we use the same dataset as in [10] to compare NeuroMHE with NeuroBEM.

Horizon $N$	10	20	40	60	80	100
Runtime [ms]	3.45	6.27	12.02	17.6	23.87	29.55

TABLE I: Runtime comparison of Algorithm 1 for different MHE horizons. The time is measured in a work station with the processor of 11th Gen Intel Core i7 – 11700K.

Table I summarizes the runtime of Algorithm 1 for different MHE horizons. The runtime is roughly linear to the horizon, and thus the algorithm can scale efficiently to a large MHE problem with a long horizon. This merit benefits from the recursive form of the analytical gradients, which makes the computational complexity of Algorithm 1 linear to  $\mathcal{O}(N)$ . Note that even when  $N = 100$ , the runtime is mere 29.55 ms, showing that our approach is computationally efficient. Based on the runtime listed in Table I, we set  $N = 10$  in training.

In Figure 3, we plot the estimation performance of NeuroMHE on the test dataset. The force estimates can converge to the ground truth data from the initial guess within about 0.1 s (see Figures 3b and 3d), thereby demonstrating fast convergence. The estimation is very accurate, especially at the challenging spikes of  $d_{fx}$  and  $d_{fy}$  (see Figure 3a and 3b). The torque estimates also show satisfactory performance, but are more noisy compared with the force estimates. To compare with NeuroBEM, we quantify the estimation performance using the Root-Mean-Square error (RMSEs) and summarize the comparison in Table II. It shows that NeuroMHE achieves 25% better overall force estimation performance (see the 5th data column) and substantially outperforms NeuroBEM with estimation error reductions of 41.2% and 49.4% in planar and vertical forces, respectively.

Method	$d_{fx}$ [N]	$d_{fy}$ [N]	$d_{\tau_{xy}}$ [Nm]	$d_{\tau_z}$ [Nm]	$d_f$ [N]	$d_{\tau}$ [Nm]
NeuroBEM	0.204	0.504	0.014	<b>0.004</b>	0.335	<b>0.012</b>
NeuroMHE	<b>0.120</b>	<b>0.255</b>	<b>0.013</b>	0.006	<b>0.251</b>	0.013

TABLE II: Comparison of estimation performance in terms of RMSEs on the test dataset. The RMSE data of NeuroBEM is obtained directly from [10]. The torque estimate of NeuroMHE in  $z$  direction is slightly worse than that of NeuroBEM. This is mainly because  $d_{\tau_z}$  is much smaller than the others, making it hard to estimate.

Due to the seamless fusion of the simple neural network with the model-based MHE estimator, another strength of our method is that it enjoys data-efficient training. NeuroBEM requires 1.26 million data points for training since it uses a relatively complicated neural network consisting of temporal-convolutional layers and MLP layers with 25k parameters. In contrast, our method uses mere 1k data points to train less than 2.5% neural network parameters (about 0.5k) and can achieve up to 49.4% better performance in the force estimation.

### B. Fast Adaptation to State-dependent Disturbance

In a second set of simulations, we aim to show that a stable NeuroMHE with fast online adaptation to the state-dependent disturbance can be trained directly from the trajectory tracking error using Algorithm 2. State-dependent disturbance exists in many aerodynamic effects such as the ground effect and the downwash effect. To this end, we synthesize the external disturbances by integrating the random walk model (2) with the state-dependent process noise. Specifically, we set  $\mathbf{w}_f \sim \mathcal{N}(0, \sigma_f)$  and  $\mathbf{w}_\tau \sim \mathcal{N}(0, \sigma_\tau)$  to be Gaussian noises and their standard deviations are updated by two polynomial functions of the quadrotor state, i.e.,  $\sigma_f = \mathbf{c}_v \text{diag}^2(\mathbf{v}) + \mathbf{c}_p \text{diag}^2(\mathbf{p}) + \mathbf{c}_f$  and  $\sigma_\tau = \mathbf{c}_\omega \text{diag}^2(\boldsymbol{\omega}) + \mathbf{c}_\Theta \text{diag}^2(\boldsymbol{\Theta}_e) + \mathbf{c}_\tau$  where  $\boldsymbol{\Theta}_e$  is the Euler angle,  $\mathbf{c}_v$ ,  $\mathbf{c}_p$ ,  $\mathbf{c}_f$ ,  $\mathbf{c}_\omega$ ,  $\mathbf{c}_\Theta$ , and  $\mathbf{c}_\tau$  are all positive definite and diagonal. Given the fact that the underactuation of quadrotors makes the horizontal disturbances much harder to compensate for than the vertical disturbance [50], we set the 3rd elements in  $\mathbf{c}_v$  and  $\mathbf{c}_p$  to be 3 times larger than the others, leading to the major disturbance force in  $z$  direction (see the arrows in Figure 4). This makes the simulation scenario similar to the downwash effect [38]. The coefficients in  $\sigma_\tau$  are set to be in the level of  $10^{-2}$  as

the aerodynamic torques are very small compared with the aerodynamic forces in practice. We generate a disturbance dataset offline for training by setting  $\mathbf{v}$ ,  $\mathbf{p}$ ,  $\boldsymbol{\Theta}_e$ , and  $\boldsymbol{\omega}$  in  $\sigma_f$  and  $\sigma_\tau$  to be the desired quadrotor states on the reference trajectory.

To further demonstrate the benefits of the adaptive tuning parameters, we compare NeuroMHE with an optimally-tuned MHE without the neural network. The latter is referred to as DMHE. It has optimal but fixed tuning parameters  $\theta^*$ , which are learned from the same disturbance dataset using gradient descent.

For the robust flight controller (21), we augment a geometric control law [43] with the current disturbance estimate from NeuroMHE as a feedforward term to compensate for the synthetic disturbance. Given the current  $\mathbf{x}_t^q$ ,  $\mathbf{u}_t$ , and  $\mathbf{d}_t$ , the quadrotor model (1) is integrated using 4th-order Runge-kutta method with a fixed time step of 10 ms to update  $\mathbf{y}_t$ , and we set  $\nu$  in the measurement (3b) to be a Gaussian noise with its fixed covariance matrix much smaller than those of  $\mathbf{w}_f$  and  $\mathbf{w}_\tau$ . The same numerical method with the same time step is also used in NeuroMHE for the state prediction. We manually tune the parameters of the geometric controller until the best performance is achieved. The number of hidden neurons is 50 and the MHE horizon is 10.

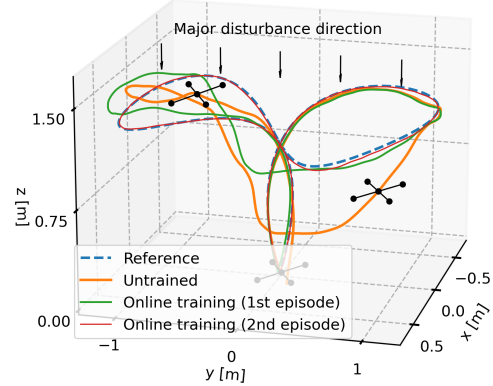
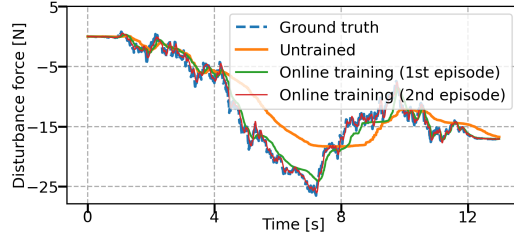


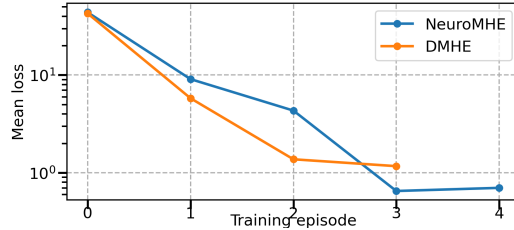
Fig. 4: Trajectory tracking performance of NeuroMHE in training. The quadrotor is controlled to take off, follow a figure-8 trajectory, and finally land at the start point. The video demos can be found at <https://youtu.be/Z68zwvhLOXE>.

We begin with visualizing the training process by a 3D plot in Figure 4. It shows that the height tracking performance is substantially improved online and the quadrotor can accurately track the reference trajectory in merely the 2nd training episode. This is mainly due to the continuously improved force estimation in  $z$  direction (see Figure 5a). We further observe in Figure 5b that although the mean loss of NeuroMHE converges slightly slower than that of DMHE, its steady value is much smaller, thereby indicating better estimation performance.

Next, we generate another disturbance dataset offline for evaluation by integrating the random walk model (2) with the same noise covariance parameters as in training. In Figure 6, we plot the inverse of the covariance parameters of  $\mathbf{w}_f$  and the weighting matrices that penalize  $\mathbf{w}_f$  in the MHE cost function (4a). The forgetting factor  $\gamma_2$  and the discounted



(a) Disturbance force in z direction in training



(b) Mean loss in training

Fig. 5: Force estimates of NeuroMHE in training and comparison of the mean loss. For the sake of comparison, the initial  $\theta_0$  of DMHE is manually tuned such that the untrained mean loss is very close to that of NeuroMHE.

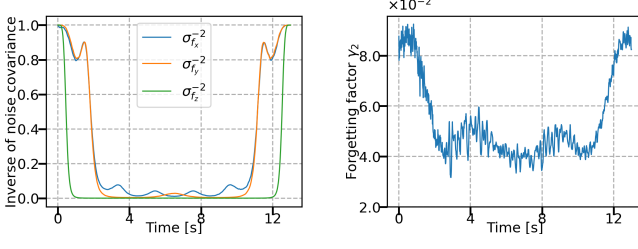
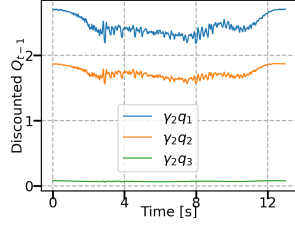
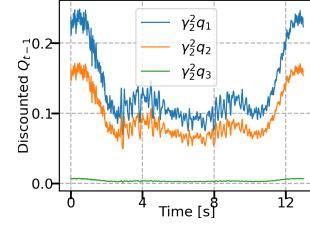
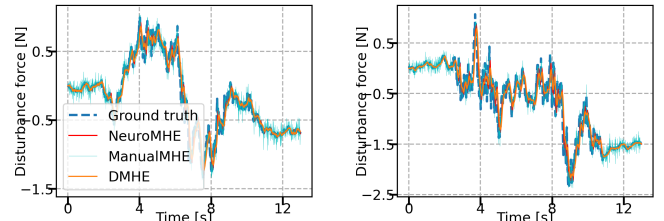
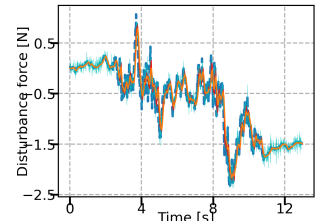
(a) Inverse of the covariance of  $w_f$ (b) Forgetting factor  $\gamma_2$ (c) Discounted  $Q_{t-1}$  with  $\gamma_2$ (d) Discounted  $Q_{t-1}$  with  $\gamma_2^2$ 

Fig. 6: Comparison of the inverse of the noise covariance parameters and the NeuroMHE weighting matrices on the unseen synthetic disturbance dataset. Here, we show two examples of the discounted  $Q_{t-1}$  with  $\gamma_2$  and  $\gamma_2^2$  respectively. The remaining  $Q_k = \gamma_2^{t-1-k} Q_{t-1}$  with  $k = t-N, \dots, t-4$  have the similar changing tendency.

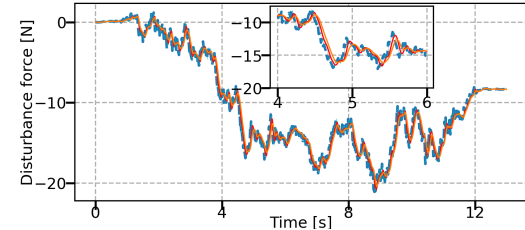
elements of  $Q_{t-1}$  change with time in a similar way to the inverse of the covariance parameters of  $w_f$ . This clearly shows that the trained neural network correctly captures the pre-defined polynomial relationship and thus makes the weighting matrices adaptive to the quadrotor state. The forgetting factor  $\gamma_1$  is much larger than  $\gamma_2$  and is stable at around 0.98, corresponding to the extremely small and fixed measurement noise covariance. For DMHE, the optimized  $\gamma_1^*$  and  $\gamma_2^*$  are 0.746 and 0.209, and the optimized  $q_{1 \sim 3}^*$  are 0.991, 0.98, and 0.566, respectively.



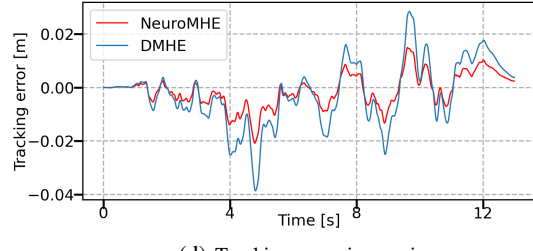
(a) Disturbance force in x axis



(b) Disturbance force in y axis



(c) Disturbance force in z axis



(d) Tracking error in z axis

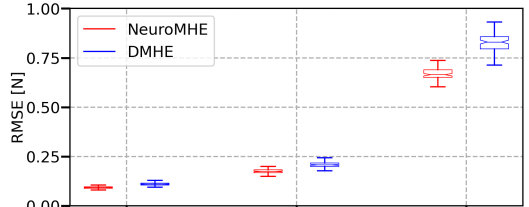
Fig. 7: Comparison of the force estimates and tracking errors in evaluation on the unseen synthetic disturbance dataset.

We compare the force estimation and trajectory tracking performances of these two methods in Figure 7. With the neural network, the time-varying  $\gamma_2$  decreases to allow for rapid changes of the force estimates in the period of 3 ~ 10 s, thus enabling NeuroMHE to accurately track the fast-changing disturbance forces during that period. In contrast, without the neural network, the force estimates of DMHE have larger estimation error and lag than those of NeuroMHE (see the zoom-in window of Figure 7c), leading to larger height tracking error shown in Figure 7d.

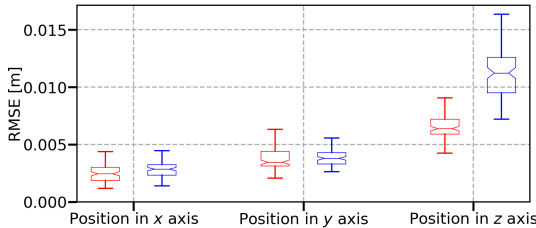
The above results provide an intuition that a small  $Q_k$  is more likely to result in good performance for the disturbance estimation. To validate this, we manually tune  $Q_k$  to be extremely small by setting  $\gamma_2$  and the diagonal elements of  $Q_{t-1}$  to be 0.01 and  $1 \times 10^{-4}$ , respectively. As shown in Figures 7a, 7b, and 7c, although the force estimation performance of this manually-tuned MHE is comparable to NeuroMHE in the period of 3 ~ 10 s, its performance degrades substantially and the force estimates are very oscillatory when the disturbance forces become slowly-varying outside that period. Such high-frequency oscillations will lead to severe stability issues for the control system. On the contrary, a well-trained NeuroMHE is more stable during the whole episode.

We further compare NeuroMHE with DMHE over 100 episodes. In each episode, the quadrotor is controlled to track the same reference trajectory as in training, and the external

disturbances are updated online by integrating the random walk model with the state-dependent noise based on the current quadrotor state. In Figure 8, we present boxplots of the RMSEs in terms of the force estimation error and the trajectory tracking error. Figure 8a shows that the estimation performance of NeuroMHE for the horizontal disturbance forces are slightly better than that of DMHE, but a significant improvement is in  $z$  direction with a 20% RMSE reduction<sup>2</sup>. Accordingly, Figure 8b shows that NeuroMHE outperforms DMHE significantly in  $z$  direction with 42% better height tracking performance.



(a) Comparison of the force estimation RMSEs



(b) Comparison of the position tracking RMSEs

Fig. 8: Boxplots of testing the estimation and trajectory tracking performance in terms of the RMSEs over 100 episodes. The 25th and 75th percentiles of each box are marked by the bottom and top edges. The line in each box denotes the median value. All the outliers are removed. Compared with the results in Table II, the RMSEs of NeuroMHE are larger as the disturbance forces are more noisy than those in the real dataset.

Overall, our simulation results indicate:

- 1) A stable NeuroMHE with fast dynamic response can be efficiently learned online from the quadrotor trajectory tracking error without the need for the ground-truth disturbance data.
- 2) The neural network can generate the optimal MHE parameters online according to the quadrotor state, rendering NeuroMHE fast adaptation to the state-dependent disturbance.

### C. Physical Experiments

We design a set of experiments on a real quadrotor to demonstrate the robustness of a NeuroMHE-augmented flight controller against various external disturbances. The proposed controller consists of a NN-parameterized Proportional-Derivative (NN-PD) controller with a gravity compensation

<sup>2</sup>Based on the boxplots in Figure 8, we further quantify the performance using the medians of the RMSEs. Specifically, we compute the performance index by  $p_{rate} = \frac{m_{DMHE} - m_{NeuroMHE}}{m_{DMHE}} \times 100\%$  where  $m_{DMHE}$  and  $m_{NeuroMHE}$  denote the medians of the RMSEs of DMHE and NeuroMHE, respectively. A positive  $p_{rate}$  represents that NeuroMHE outperforms DMHE.

(defined as a baseline controller) and a feedforward term from NeuroMHE for counteracting the disturbance. We evaluate the proposed controller in two experiments: 1) a step disturbance force by releasing a payload, and 2) a complex time-varying aerodynamic force by the downwash effect. The setup of hardware platform required is outlined in Figure 9. The training

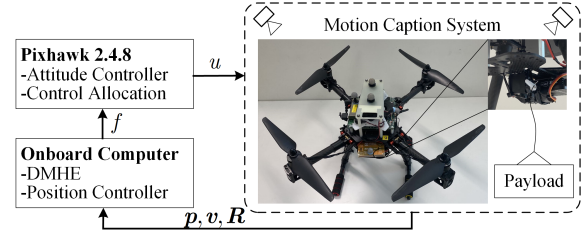


Fig. 9: Overview of the hardware components where the quadrotor weighs 1.8 kg and the on-board computer running ROS melodic is the 64-bit Intel nuc with the processor of Intel Core i7-5557U CPU.

process is that the quadrotor with a payload tethered to it iteratively takes off in simulation. We set the payload mass to be a square-wave signal and its value is randomly set at the beginning. Since the force estimation and position dynamics are the primary concern in the experiment,  $\theta$  consists of 20 elements. The number of hidden neurons is 50. The trained NeuroMHE and NN-PD controller are deployed to the real quadrotor without extra tuning.

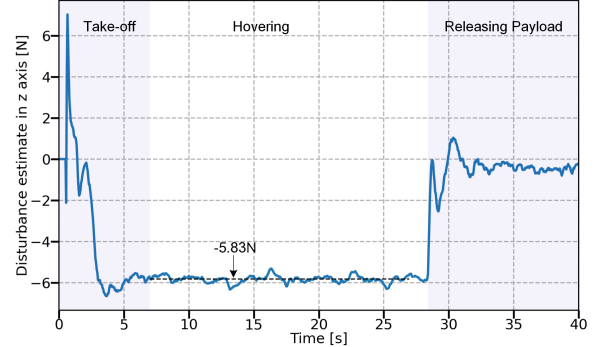


Fig. 10: Estimate of disturbance force in  $z$ -direction posed by the payload in the East-North-Up inertial frame. The average of the estimated force is  $-5.83$  N which is accurate compared to the ground truth of  $-5.87$  N. The payload is released at around 28 s and NeuroMHE can respond to this sudden change rapidly. The initial estimated force mainly comes from the ground effect which provides the quadrotor with extra lift.

Before the fly tests, we first use a payload of known weighting (600 g) to calibrate NeuroMHE in order to remove any bias caused by inaccurate modeling. The first experiment is to test the dynamic response of NeuroMHE to a step-disturbance. To this end, we make the quadrotor take off with the payload and release it once hovering at the 1.5 m height setpoint. The payload is tethered to the quadrotor with tether length of 0.4 m. At around 28 s in Figure 10, the payload is released and NeuroMHE responds to this sudden change quickly with a rising time less than 0.5 s. The external force posed by the payload (during about 7 to 28 s in Figure 10) is estimated by NeuroMHE to be  $-5.83$  N with a standard deviation of 0.03 N. This is a satisfactory estimation compared

with the true weight of  $0.6 \text{ kg} \times 9.78 \text{ m s}^{-2} \approx 5.87 \text{ N}$  using the local gravitational acceleration in Singapore.

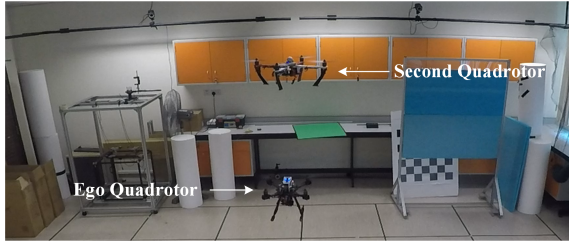


Fig. 11: Illustration of the downwash experiment. The second quadrotor hovers at about 0.7 m above the ego one, which begins at 30 s to produce the downwash effect. The width of the second quadrotor is 0.3 m.

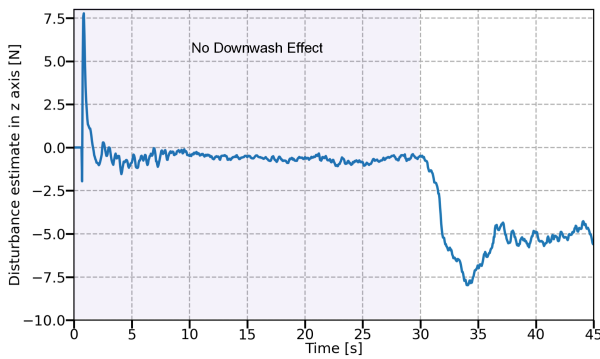


Fig. 12: Estimation of aerodynamic disturbance force caused by the downwash effect. Same as Figure 10, the initial estimated force mainly comes from the ground effect which provides the quadrotor with extra lift. The small steady disturbance of about 0.7 N during 17 to 30 s is caused by the airflow interaction between these two quadrotors.

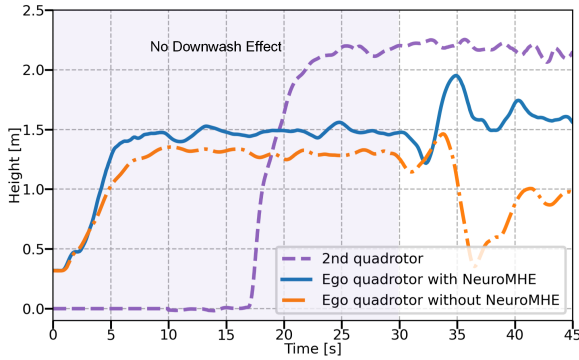


Fig. 13: Comparison of hovering under the downwash effect between the NN-PD baseline controller and the proposed controller. The ego quadrotor is programmed to take off without the payload and hover at 1.5 m height setpoint. After that, we make the second quadrotor fly and hover at 0.7 m above the ego one, which begins at around 30 s. Because only the disturbance forces are compensated, the proposed position controller takes time to suppress the oscillation due to the coupling with the perturbed rotational dynamics.

The second experiment is to test the robustness of the proposed method against the downwash effect. Passing through the downwash airflow generated by another quadrotor can cause a significant loss of lift (see Figure 12) and thus leads to catastrophic failure. We program the ego quadrotor (see the setup in Figure 9) to automatically take off and hover at

1.5 m, and then let a second quadrotor hover at 0.8 m above the ego one (see Figure 11, which begins at around 30 s in Figure 13). We can see from Figure 13 that the NeuroMHE compensation enables the ego quadrotor to maintain at the desired height after a mild oscillation with a small amplitude. On the contrary, if we use the baseline controller alone, there is a severe oscillation after 30 s and the steady height evidently deviates from the desired one. Figure 13 also shows that the second quadrotor under the PID control cannot maintain at the desired 0.8 m height setpoint above the ego one with a steady state tracking error of about 0.1 m due to the ceiling effect. Therefore, it is necessary to incorporate NeuroMHE into a flight controller for improving the robustness of quadrotor against these challenging disturbances.

## VIII. CONCLUSION

This paper proposes a novel estimator named NeuroMHE to accurately estimate the external disturbances for different flight scenarios. Our key insight is that NeuroMHE can efficiently tune its parameters modeled by a neural network online from the trajectory tracking error to achieve adaptive and optimal estimation performance. At the core of our approach are the analytical gradients of the MHE estimates with respect to the tuning parameters, which are in a recursive form via a Kalman filter and enable a seamless embedding of MHE into the neural network for highly effective learning. Comparing with state-of-the-art in extensive simulations, we show that our method reduces force estimation errors by up to 49.4% with much less training data and can adapt to the state-dependent disturbance with up to 42% better trajectory tracking performance. Experiments on a real quadrotor further demonstrate that a baseline controller augmented with NeuroMHE can significantly improve the robustness against challenging disturbances such as the sudden payload change and the downwash effect.

There are several exciting directions for future work. In particular, we are interested in providing a theoretical stability guarantee for NeuroMHE, which will further improve its applicability to various safety-crucial robotic systems. In addition, developing second-order learning algorithms to speed up the online training process of NeuroMHE is also a promising avenue for future robust adaptive control.

## ACKNOWLEDGEMENT

We are grateful to Leonard Bauersfeld for many valuable discussions regarding his work on NeuroBEM and help on using the flight dataset.

## REFERENCES

- [1] B. Wang, Z. Ma, S. Lai, L. Zhao, and T. H. Lee, "Differentiable moving horizon estimation for robust flight control," in *2021 60th IEEE Conference on Decision and Control (CDC)*. IEEE, 2021, pp. 3563–3568.
- [2] W. Hönig, J. A. Preiss, T. S. Kumar, G. S. Sukhatme, and N. Ayanian, "Trajectory planning for quadrotor swarms," *IEEE Transactions on Robotics*, vol. 34, no. 4, pp. 856–869, 2018.
- [3] S. Gupte, P. I. T. Mohandas, and J. M. Conrad, "A survey of quadrotor unmanned aerial vehicles," in *2012 Proceedings of IEEE Southeastcon*. IEEE, 2012, pp. 1–6.

- [4] M. Brunner, L. Giacomini, R. Siegwart, and M. Tognon, "Energy tank-based policies for robust aerial physical interaction with moving objects," *arXiv preprint arXiv:2202.06755*, 2022.
- [5] J. Geng and J. W. Langelaan, "Cooperative transport of a slung load using load-leading control," *Journal of Guidance, Control, and Dynamics*, vol. 43, no. 7, pp. 1313–1331, 2020.
- [6] B. E. Jackson, T. A. Howell, K. Shah, M. Schwager, and Z. Manchester, "Scalable cooperative transport of cable-suspended loads with uavs using distributed trajectory optimization," *IEEE Robotics and Automation Letters*, vol. 5, no. 2, pp. 3368–3374, 2020.
- [7] N. Michael, D. Mellinger, Q. Lindsey, and V. Kumar, "The grasp multiple micro-uav testbed," *IEEE Robotics & Automation Magazine*, vol. 17, no. 3, pp. 56–65, 2010.
- [8] C. Powers, D. Mellinger, A. Kushleyev, B. Kothmann, and V. Kumar, "Influence of aerodynamics and proximity effects in quadrotor flight," in *Experimental robotics*. Springer, 2013, pp. 289–302.
- [9] Y. Naka and A. Kagami, "Coanda effect of a propeller airflow and its aerodynamic impact on the thrust," *Journal of Fluid Science and Technology*, vol. 15, no. 3, pp. JFST0016–JFST0016, 2020.
- [10] L. Bauersfeld, E. Kaufmann, P. Foehn, S. Sun, and D. Scaramuzza, "Neurobem: Hybrid aerodynamic quadrotor model," *arXiv preprint arXiv:2106.08015*, 2021.
- [11] G. Shi, W. Höning, X. Shi, Y. Yue, and S.-J. Chung, "Neural-swarm2: Planning and control of heterogeneous multirotor swarms using learned interactions," *IEEE Transactions on Robotics*, 2021.
- [12] S. Belkhale, R. Li, G. Kahn, R. McAllister, R. Calandra, and S. Levine, "Model-based meta-reinforcement learning for flight with suspended payloads," *IEEE Robotics and Automation Letters*, vol. 6, no. 2, pp. 1471–1478, 2021.
- [13] F. Ruggiero, J. Cacace, H. Sadeghian, and V. Lippiello, "Impedance control of vtol uavs with a momentum-based external generalized forces estimator," in *2014 IEEE International Conference on Robotics and Automation (ICRA)*, 2014, pp. 2093–2099.
- [14] B. Yüksel, C. Secchi, H. H. Bülthoff, and A. Franchi, "A nonlinear force observer for quadrotors and application to physical interactive tasks," in *2014 IEEE/ASME international conference on advanced intelligent mechatronics*. IEEE, 2014, pp. 433–440.
- [15] T. Tomić and S. Haddadin, "A unified framework for external wrench estimation, interaction control and collision reflexes for flying robots," in *2014 IEEE/RSJ International Conference on Intelligent Robots and Systems*. IEEE, 2014, pp. 4197–4204.
- [16] K. Bodie, M. Brunner, M. Pantic, S. Walser, P. Pfändler, U. Angst, R. Siegwart, and J. Nieto, "Active interaction force control for contact-based inspection with a fully actuated aerial vehicle," *IEEE Transactions on Robotics*, vol. 37, no. 3, pp. 709–722, 2021.
- [17] C. D. McKinnon and A. P. Schoellig, "Estimating and reacting to forces and torques resulting from common aerodynamic disturbances acting on quadrotors," *Robotics and Autonomous Systems*, vol. 123, p. 103314, 2020.
- [18] A. Punjani and P. Abbeel, "Deep learning helicopter dynamics models," in *2015 IEEE International Conference on Robotics and Automation (ICRA)*. IEEE, 2015, pp. 3223–3230.
- [19] N. Mohajerin, M. Mozifian, and S. Waslander, "Deep learning a quadrotor dynamic model for multi-step prediction," in *2018 IEEE International Conference on Robotics and Automation (ICRA)*. IEEE, 2018, pp. 2454–2459.
- [20] M. Diehl, H. J. Ferreau, and N. Haverbeke, "Efficient numerical methods for nonlinear mpc and moving horizon estimation," in *Nonlinear model predictive control*. Springer, 2009, pp. 391–417.
- [21] S. S. Mansouri, H. Jafari, and G. Nikolakopoulos, "External force estimation based on nonlinear moving horizon estimation for mav navigation," in *2020 European Control Conference (ECC)*, 2020, pp. 1312–1317.
- [22] A. Wenz and T. A. Johansen, "Moving horizon estimation of air data parameters for uavs," *IEEE Transactions on Aerospace and Electronic Systems*, vol. 56, no. 3, pp. 2101–2121, 2019.
- [23] M. Osman, M. W. Mehrez, M. A. Daoud, A. Hussein, S. Jeon, and W. Melek, "A generic multi-sensor fusion scheme for localization of autonomous platforms using moving horizon estimation," *Transactions of the Institute of Measurement and Control*, vol. 43, no. 15, pp. 3413–3427, 2021.
- [24] A. Eltrabyly, D. Ichalal, and S. Mammar, "Quadcopter trajectory tracking in the presence of 4 faulty actuators: A nonlinear mhe and mpc approach," *IEEE Control Systems Letters*, vol. 6, pp. 2024–2029, 2021.
- [25] Y. Hu, C. Gao, and W. Jing, "Joint state and parameter estimation for hypersonic glide vehicles based on moving horizon estimation via carleman linearization," *Aerospace*, vol. 9, no. 4, p. 217, 2022.
- [26] D. G. Robertson, J. H. Lee, and J. B. Rawlings, "A moving horizon-based approach for least-squares estimation," *AIChE Journal*, vol. 42, no. 8, pp. 2209–2224, 1996.
- [27] A. Y. Aravkin and J. V. Burke, "Smoothing dynamic systems with state-dependent covariance matrices," in *53rd IEEE Conference on Decision and Control*. IEEE, 2014, pp. 3382–3387.
- [28] C. Nguyen Van, "State estimation based on sigma point kalman filter for suspension system in presence of road excitation influenced by velocity of the car," *Journal of Control Science and Engineering*, vol. 2019, 2019.
- [29] B. Amos and J. Z. Kolter, "OptNet: Differentiable optimization as a layer in neural networks," in *International Conference on Machine Learning*. PMLR, 2017, pp. 136–145.
- [30] B. Amos, I. D. J. Rodriguez, J. Sacks, B. Boots, and J. Z. Kolter, "Differentiable mpc for end-to-end planning and control," in *Proceedings of the 32nd International Conference on Neural Information Processing Systems*, 2018, pp. 8299–8310.
- [31] W. Jin, Z. Wang, Z. Yang, and S. Mou, "Pontryagin differentiable programming: An end-to-end learning and control framework," *Advances in Neural Information Processing Systems*, vol. 33, 2020.
- [32] W. Jin, S. Mou, and G. J. Pappas, "Safe pontryagin differentiable programming," *Advances in Neural Information Processing Systems*, vol. 34, pp. 16 034–16 050, 2021.
- [33] H. N. Esfahani, A. B. Kordabad, and S. Gros, "Reinforcement learning based on mpc/mhe for unmodeled and partially observable dynamics," in *2021 American Control Conference (ACC)*, 2021, pp. 2121–2126.
- [34] S. Muntwiler, K. P. Wabersich, and M. N. Zeilinger, "Learning-based moving horizon estimation through differentiable convex optimization layers," *arXiv preprint arXiv:2109.03962*, 2021.
- [35] A. Alessandri, M. Baglietto, G. Battistelli, and V. Zavala, "Advances in moving horizon estimation for nonlinear systems," in *49th IEEE Conference on Decision and Control (CDC)*. IEEE, 2010, pp. 5681–5688.
- [36] C. V. Rao, J. B. Rawlings, and D. Q. Mayne, "Constrained state estimation for nonlinear discrete-time systems: Stability and moving horizon approximations," *IEEE transactions on automatic control*, vol. 48, no. 2, pp. 246–258, 2003.
- [37] N. Sydney, B. Smyth, and D. A. Paley, "Dynamic control of autonomous quadrotor flight in an estimated wind field," in *52nd IEEE Conference on Decision and Control*. IEEE, 2013, pp. 3609–3616.
- [38] C.-C. Chen and H. H. Liu, "Model of uav and downwash for multi-uav path planning," in *AIAA SCITECH 2022 Forum*, 2022, p. 0757.
- [39] P. Sanchez-Cuevas, G. Heredia, and A. Ollero, "Characterization of the aerodynamic ground effect and its influence in multirotor control," *International Journal of Aerospace Engineering*, vol. 2017, 2017.
- [40] G. Shi, W. Höning, Y. Yue, and S.-J. Chung, "Neural-swarm: Decentralized close-proximity multirotor control using learned interactions," in *2020 IEEE International Conference on Robotics and Automation (ICRA)*. IEEE, 2020, pp. 3241–3247.
- [41] J. A. Andersson, J. Gillis, G. Horn, J. B. Rawlings, and M. Diehl, "Casadi: a software framework for nonlinear optimization and optimal control," *Mathematical Programming Computation*, vol. 11, no. 1, pp. 1–36, 2019.
- [42] H. Cox, "Estimation of state variables for noisy dynamic systems," Ph.D. dissertation, Massachusetts Institute of Technology, 1963.
- [43] T. Lee, M. Leok, and N. H. McClamroch, "Geometric tracking control of a quadrotor UAV on  $SE(3)$ ," in *49th IEEE conference on decision and control (CDC)*. IEEE, 2010, pp. 5420–5425.
- [44] A. Forsgren, P. E. Gill, and M. H. Wright, "Interior methods for nonlinear optimization," *SIAM review*, vol. 44, no. 4, pp. 525–597, 2002.
- [45] A. Krizhevsky, I. Sutskever, and G. E. Hinton, "Imagenet classification with deep convolutional neural networks," *Advances in neural information processing systems*, vol. 25, pp. 1097–1105, 2012.
- [46] P. Kühl, M. Diehl, T. Kraus, J. P. Schlöder, and H. G. Bock, "A real-time algorithm for moving horizon state and parameter estimation," *Computers & chemical engineering*, vol. 35, no. 1, pp. 71–83, 2011.
- [47] T. Kraus, H. J. Ferreau, E. Kayacan, H. Ramon, J. De Baerdemaeker, M. Diehl, and W. Saeys, "Moving horizon estimation and nonlinear model predictive control for autonomous agricultural vehicles," *Computers and electronics in agriculture*, vol. 98, pp. 25–33, 2013.
- [48] A. Paszke, S. Gross, F. Massa, A. Lerer, J. Bradbury, G. Chanan, T. Killeen, Z. Lin, N. Gimelshein, L. Antiga *et al.*, "Pytorch: An imperative style, high-performance deep learning library," *Advances in neural information processing systems*, vol. 32, pp. 8026–8037, 2019.
- [49] D. P. Kingma and J. Ba, "Adam: A method for stochastic optimization," *arXiv preprint arXiv:1412.6980*, 2014.

[50] D. Hanover, P. Foehn, S. Sun, E. Kaufmann, and D. Scaramuzza, “Performance, precision, and payloads: Adaptive nonlinear mpc for quadrotors,” *IEEE Robotics and Automation Letters*, vol. 7, no. 2, pp. 690–697, 2021.

## APPENDIX

### A. Proof of Lemma 1

For the auxiliary MHE system (16), we define the following Lagrangian

$$\mathcal{L}_2 = \frac{1}{2} \text{Tr} \left\| \mathbf{X}_{t-N} - \hat{\mathbf{X}}_{t-N} \right\|_{\mathbf{P}}^2 + \bar{\mathcal{L}}_2, \quad (28)$$

where

$$\begin{aligned} \bar{\mathcal{L}}_2 = & \text{Tr} \sum_{k=t-N}^t \left( \frac{1}{2} \mathbf{X}_k^T \bar{\mathbf{L}}_k^{xx} \mathbf{X}_k + \mathbf{W}_k^T \mathbf{L}_k^{wx} \mathbf{X}_k \right) \\ & + \text{Tr} \sum_{k=t-N}^{t-1} \left( \frac{1}{2} \mathbf{W}_k^T \mathbf{L}_k^{ww} \mathbf{W}_k + (\mathbf{L}_k^{w\theta})^T \mathbf{W}_k \right) \\ & + \text{Tr} \sum_{k=t-N}^t \left( (\mathbf{L}_k^{x\theta})^T \mathbf{X}_k \right) \\ & + \text{Tr} \sum_{k=t-N}^{t-1} \mathbf{\Lambda}_k^T (\mathbf{X}_{k+1} - \mathbf{F}_k \mathbf{X}_k - \mathbf{G}_k \mathbf{W}_k). \end{aligned}$$

The optimal estimates  $\hat{\mathbf{X}}$  and  $\hat{\mathbf{W}}$ , together with the new optimal dual variables  $\mathbf{\Lambda}^* = \{\mathbf{\Lambda}_k^* \}_{k=t-N}^{t-1}$ , satisfy the following KKT conditions:

$$\begin{aligned} \nabla_{\mathbf{X}_{t-N}} \mathcal{L}_2 = & (\mathbf{P} + \bar{\mathbf{L}}_{t-N}^{xx}) \hat{\mathbf{X}}_{t-N|t} - \mathbf{P} \hat{\mathbf{X}}_{t-N} + \mathbf{L}_{t-N}^{x\theta} \\ & + \mathbf{L}_{t-N}^{wx} \hat{\mathbf{W}}_{t-N|t} - \mathbf{F}_{t-N}^T \mathbf{\Lambda}_{t-N}^* = \mathbf{0}, \end{aligned} \quad (29a)$$

$$\begin{aligned} \nabla_{\mathbf{X}_k} \mathcal{L}_2 = & \bar{\mathbf{L}}_k^{xx} \hat{\mathbf{X}}_{k|t} + \mathbf{L}_k^{wx} \hat{\mathbf{W}}_{k|t} - \mathbf{F}_k^T \mathbf{\Lambda}_k^* + \mathbf{\Lambda}_{k-1}^* \\ & + \mathbf{L}_k^{x\theta} = \mathbf{0}, \quad k = t-N+1, \dots, t, \end{aligned} \quad (29b)$$

$$\begin{aligned} \nabla_{\mathbf{W}_k} \mathcal{L}_2 = & \mathbf{L}_k^{wx} \hat{\mathbf{X}}_{k|t} + \mathbf{L}_k^{ww} \hat{\mathbf{W}}_{k|t} - \mathbf{G}_k^T \mathbf{\Lambda}_k^* \\ & + \mathbf{L}_k^{w\theta} = \mathbf{0}, \quad k = t-N, \dots, t-1, \end{aligned} \quad (29c)$$

$$\begin{aligned} \nabla_{\mathbf{\Lambda}_k} \mathcal{L}_2 = & \hat{\mathbf{X}}_{k+1|t} - \mathbf{F}_k \hat{\mathbf{X}}_{k|t} - \mathbf{G}_k \hat{\mathbf{W}}_{k|t} = \mathbf{0}, \\ & k = t-N, \dots, t-1. \end{aligned} \quad (29d)$$

The above equations (29) are the same as the differential KKT conditions (13), and thus (15) holds. This completes the proof.

### B. Proof of Lemma 2

Given all the required data collected in the horizon from  $t-N$  to  $t$ , we prove Lemma 2 by forward induction.

First, consider the simplest case where only the data at  $t-N$  is used and the auxiliary MHE system (16) reduces to a Kalman filter. The goal is to obtain the state estimate  $\hat{\mathbf{X}}_{t-N|t-N}^{\text{KF}}$ . This can be achieved by solving the KKT condition (29a), which however requires  $\hat{\mathbf{W}}_{t-N|t-N}$  and  $\mathbf{\Lambda}_{t-N}^*$ . Because there is no need to predict the system state, the KKT condition for the dynamics equality constraint (29d) can be removed and thus  $\mathbf{\Lambda}_{t-N}^* = \mathbf{0}$ . It follows that we can express  $\hat{\mathbf{W}}_{t-N|t-N}$  in terms of  $\hat{\mathbf{X}}_{t-N|t-N}^{\text{KF}}$  from

(29c). Plugging the resulting  $\hat{\mathbf{W}}_{t-N|t-N}$  into (29a) and using  $\bar{\mathbf{X}}_{t-N} = \mathbf{P}_{t-N} \mathbf{T}_{t-N} + \hat{\mathbf{X}}_{t-N}$  yield

$$\hat{\mathbf{X}}_{t-N|t-N}^{\text{KF}} = \bar{\mathbf{X}}_{t-N} + \mathbf{P}_{t-N} \mathbf{S}_{t-N} \hat{\mathbf{X}}_{t-N|t-N}^{\text{KF}}. \quad (30)$$

The above equation is equivalent to the following form:

$$\begin{aligned} (\mathbf{I} - \mathbf{P}_{t-N} \mathbf{S}_{t-N}) \hat{\mathbf{X}}_{t-N|t-N}^{\text{KF}} = & (\mathbf{I} - \mathbf{P}_{t-N} \mathbf{S}_{t-N}) \bar{\mathbf{X}}_{t-N} \\ & + \mathbf{P}_{t-N} \mathbf{S}_{t-N} \bar{\mathbf{X}}_{t-N}. \end{aligned} \quad (31)$$

Define  $\mathbf{C}_{t-N} = (\mathbf{I} - \mathbf{P}_{t-N} \mathbf{S}_{t-N})^{-1} \mathbf{P}_{t-N}$ . We can therefore simplify (31) to

$$\hat{\mathbf{X}}_{t-N|t-N}^{\text{KF}} = (\mathbf{I} + \mathbf{C}_{t-N} \mathbf{S}_{t-N}) \bar{\mathbf{X}}_{t-N} \quad (32)$$

which is exactly the initial condition (17a).

Next, we move one step forward. Consider the case where the data at  $t-N$  and  $t-N+1$  is used and the goal is to obtain the sequence  $\{\hat{\mathbf{X}}_{t-N|t-N+1}, \hat{\mathbf{X}}_{t-N+1|t-N+1}\}$ . From (29c), we solve for  $\hat{\mathbf{W}}_{t-N|t-N+1}$  in terms of  $\hat{\mathbf{X}}_{t-N|t-N+1}$  and  $\mathbf{\Lambda}_{t-N}^*$ :

$$\begin{aligned} \hat{\mathbf{W}}_{t-N|t-N+1} = & (\mathbf{L}_{t-N}^{ww})^{-1} (\mathbf{G}_{t-N}^T \mathbf{\Lambda}_{t-N}^* \\ & - \mathbf{L}_{t-N}^{wx} \hat{\mathbf{X}}_{t-N|t-N+1} - \mathbf{L}_{t-N}^{w\theta}). \end{aligned} \quad (33)$$

Using the above equation, we can rewrite (29a) as

$$\begin{aligned} \hat{\mathbf{X}}_{t-N|t-N+1} = & \bar{\mathbf{X}}_{t-N} + \mathbf{P}_{t-N} \mathbf{S}_{t-N} \hat{\mathbf{X}}_{t-N|t-N+1} \\ & + \mathbf{P}_{t-N} \bar{\mathbf{F}}_{t-N}^T \mathbf{\Lambda}_{t-N}^*. \end{aligned} \quad (34)$$

An equivalent expression similar to (31) can be obtained for (34). With  $\mathbf{C}_{t-N}$  defined above, we can rewrite the equivalent expression of (34) as

$$\begin{aligned} \hat{\mathbf{X}}_{t-N|t-N+1} = & (\mathbf{I} + \mathbf{C}_{t-N} \mathbf{S}_{t-N}) \bar{\mathbf{X}}_{t-N} \\ & + \mathbf{C}_{t-N} \bar{\mathbf{F}}_{t-N}^T \mathbf{\Lambda}_{t-N}^*. \end{aligned} \quad (35)$$

Comparing with (32), we can reduce (35) to

$$\hat{\mathbf{X}}_{t-N|t-N+1} = \hat{\mathbf{X}}_{t-N|t-N}^{\text{KF}} + \mathbf{C}_{t-N} \bar{\mathbf{F}}_{t-N}^T \mathbf{\Lambda}_{t-N}^*. \quad (36)$$

Note that we have  $\mathbf{\Lambda}_{t-N+1}^* = \mathbf{0}$  as there is only one dynamics equality constraint associated with  $\mathbf{\Lambda}_{t-N}^*$ . Using  $\mathbf{\Lambda}_{t-N+1}^* = \mathbf{0}$  and (33), we can solve for  $\mathbf{\Lambda}_{t-N}^*$  from (29b) as:

$$\mathbf{\Lambda}_{t-N}^* = \mathbf{S}_{t-N+1} \hat{\mathbf{X}}_{t-N+1|t-N+1} + \mathbf{T}_{t-N+1}. \quad (37)$$

Plugging (33) and (36) into the dynamics equality constraint (29d) yields the state prediction

$$\begin{aligned} \hat{\mathbf{X}}_{t-N+1|t-N+1} = & \bar{\mathbf{F}}_{t-N} \hat{\mathbf{X}}_{t-N|t-N} \\ & - \mathbf{G}_{t-N} (\mathbf{L}_{t-N}^{ww})^{-1} \mathbf{L}_{t-N}^{w\theta} \\ & + \bar{\mathbf{F}}_{t-N} \mathbf{C}_{t-N} \bar{\mathbf{F}}_{t-N}^T \mathbf{\Lambda}_{t-N}^* \\ & + \mathbf{G}_{t-N} (\mathbf{L}_{t-N}^{ww})^{-1} \mathbf{G}_{t-N}^T \mathbf{\Lambda}_{t-N}^*. \end{aligned} \quad (38)$$

Define

$$\hat{\mathbf{X}}_{t-N+1|t-N} = \bar{\mathbf{F}}_{t-N} \hat{\mathbf{X}}_{t-N|t-N} - \mathbf{G}_{t-N} (\mathbf{L}_{t-N}^{ww})^{-1} \mathbf{L}_{t-N}^{w\theta} \quad (39)$$

and

$$\mathbf{P}_{t-N+1} = \bar{\mathbf{F}}_{t-N} \mathbf{C}_{t-N} \bar{\mathbf{F}}_{t-N}^T + \mathbf{G}_{t-N} (\mathbf{L}_{t-N}^{ww})^{-1} \mathbf{G}_{t-N}^T. \quad (40)$$

Using (39) and (40), we can rewrite (38) as

$$\hat{\mathbf{X}}_{t-N+1|t-N+1} = \hat{\mathbf{X}}_{t-N+1|t-N} + \mathbf{P}_{t-N+1} \Lambda_{t-N}^*. \quad (41)$$

Plugging (37) into (41) yields

$$\begin{aligned} \hat{\mathbf{X}}_{t-N+1|t-N+1} &= \hat{\mathbf{X}}_{t-N+1|t-N} \\ &+ \mathbf{P}_{t-N+1} \mathbf{S}_{t-N+1} \hat{\mathbf{X}}_{t-N+1|t-N+1} \\ &+ \mathbf{P}_{t-N+1} \mathbf{T}_{t-N+1}. \end{aligned} \quad (42)$$

After a procedure similar to the one used for (30), we can obtain an equivalent equation of (42) similar to (31). Let

$$\mathbf{C}_{t-N+1} = (\mathbf{I} - \mathbf{P}_{t-N+1} \mathbf{S}_{t-N+1})^{-1} \mathbf{P}_{t-N+1}, \quad (43)$$

then we can simplify the equivalent equation of (42) to

$$\begin{aligned} \hat{\mathbf{X}}_{t-N+1|t-N+1} &= (\mathbf{I} + \mathbf{C}_{t-N+1} \mathbf{S}_{t-N+1}) \hat{\mathbf{X}}_{t-N+1|t-N} \\ &+ \mathbf{C}_{t-N+1} \mathbf{T}_{t-N+1}. \end{aligned} \quad (44)$$

Equations (36), (40), (43), and (44) are similar in structure to equations (20), (18b), (18c), and (18d) presented in Lemma 2. In particular, the relation (36) is the key to the general solution, as we will show shortly.

Finally, consider the general case where all the data in the horizon is used and the goal is to obtain the complete sequence  $\{\hat{\mathbf{X}}_{k|t}\}_{k=t-N}^t$ . We aim to show that if (20) is satisfied by  $\hat{\mathbf{X}}_{k|t}$ , then it also holds for  $\hat{\mathbf{X}}_{k+1|t}$ . Before proceeding to the proof, let us first combine (29c) and (29d) to eliminate  $\hat{\mathbf{W}}_{k|t}$ :

$$\hat{\mathbf{X}}_{k+1|t} = \bar{\mathbf{F}}_k \hat{\mathbf{X}}_{k|t} - \mathbf{G}_k (\mathbf{L}_k^{ww})^{-1} \mathbf{L}_k^{w\theta} + \mathbf{G}_k (\mathbf{L}_k^{ww})^{-1} \mathbf{G}_k^T \Lambda_k^*. \quad (45)$$

Similarly, by substituting for  $\hat{\mathbf{W}}_{k|t}$  in (29b), we obtain

$$\Lambda_{k-1}^* = \bar{\mathbf{F}}_k \Lambda_k^* + \mathbf{S}_k \hat{\mathbf{X}}_{k|t} + \mathbf{T}_k. \quad (46)$$

Suppose that  $\hat{\mathbf{X}}_{k|t}$  satisfies (20) for  $k \in [t-N, t-1]$ . Then, from (45), we have

$$\begin{aligned} \hat{\mathbf{X}}_{k+1|t} &= \bar{\mathbf{F}}_k \hat{\mathbf{X}}_{k|k}^{\text{KF}} - \mathbf{G}_k (\mathbf{L}_k^{ww})^{-1} \mathbf{L}_k^{w\theta} \\ &+ \left[ \bar{\mathbf{F}}_k \mathbf{C}_k \bar{\mathbf{F}}_k^T + \mathbf{G}_k (\mathbf{L}_k^{ww})^{-1} \mathbf{G}_k^T \right] \Lambda_k^*. \end{aligned} \quad (47)$$

Using (18a), we can simplify (47) to

$$\hat{\mathbf{X}}_{k+1|t} = \hat{\mathbf{X}}_{k+1|k} + \left[ \bar{\mathbf{F}}_k \mathbf{C}_k \bar{\mathbf{F}}_k^T + \mathbf{G}_k (\mathbf{L}_k^{ww})^{-1} \mathbf{G}_k^T \right] \Lambda_k^*. \quad (48)$$

Substituting  $\mathbf{P}_{k+1}$  from (18b) and  $\Lambda_k^*$  from (46), we obtain

$$\begin{aligned} \hat{\mathbf{X}}_{k+1|t} &= \hat{\mathbf{X}}_{k+1|k} + \mathbf{P}_{k+1} \mathbf{T}_{k+1} + \mathbf{P}_{k+1} \mathbf{S}_{k+1} \hat{\mathbf{X}}_{k+1|t} \\ &+ \mathbf{P}_{k+1} \bar{\mathbf{F}}_{k+1} \Lambda_{k+1}^*. \end{aligned} \quad (49)$$

The above equation is equivalent to the following form:

$$\begin{aligned} (\mathbf{I} - \mathbf{P}_{k+1} \mathbf{S}_{k+1}) \hat{\mathbf{X}}_{k+1|t} &= (\mathbf{I} - \mathbf{P}_{k+1} \mathbf{S}_{k+1}) \hat{\mathbf{X}}_{k+1|k} \\ &+ \mathbf{P}_{k+1} \mathbf{S}_{k+1} \hat{\mathbf{X}}_{k+1|k} \\ &+ \mathbf{P}_{k+1} \mathbf{T}_{k+1} + \mathbf{P}_{k+1} \bar{\mathbf{F}}_{k+1} \Lambda_{k+1}^*. \end{aligned} \quad (50)$$

Substituting  $\mathbf{C}_{k+1}$  from (18c) and  $\hat{\mathbf{X}}_{k+1|k+1}^{\text{KF}}$  from (18d), we obtain the desired relation as below:

$$\hat{\mathbf{X}}_{k+1|t} = \hat{\mathbf{X}}_{k+1|k+1}^{\text{KF}} + \mathbf{C}_{k+1} \bar{\mathbf{F}}_{k+1}^T \Lambda_{k+1}^*. \quad (51)$$

This completes the proof.